NASA TECHNICAL NOTE

NASA TN D-4903

NASA TN D-4903

A COMPARISON OF A CLASS OF EARTH-MOON ORBITS WITH A CLASS OF ROTATING KEPLER ORBITS

by R. F. Hoelker and B. P. Winston

Electronics Research Center
Cambridge, Mass.

NATIONAL AERONAUTICS AND SPACE ADMINISTRATION • WASHINGTON, D. C. • NOVEMBER 1968

NASA TN D-4903

A COMPARISON OF A CLASS OF EARTH-MOON ORBITS WITH A CLASS OF ROTATING KEPLER ORBITS

By R. F. Hoelker and B. P. Winston

Electronics Research Center
Cambridge, Mass.

NATIONAL AERONAUTICS AND SPACE ADMINISTRATION

For sale by the Clearinghouse for Federal Scientific and Technical Information
Springfield, Virginia 22151 – CFSTI price $3.00

A COMPARISON OF A CLASS OF EARTH-MOON ORBITS WITH A CLASS OF ROTATING KEPLER ORBITS

By R. F. Hoelker and B. P. Winston
Electronics Research Center

SUMMARY

In two concurrent series of graphs, a class of orbits in the Earth-Moon (E-M) field and a class of Kepler orbits in rotating coordinates are depicted and compared.

A general discussion of characteristics of rotating Kepler orbits is included.

The model used for the E-M orbits is that of the restricted problem of three bodies. The orbits of the class depicted originate at the E-M line, half of the E-M distance beyond the moon with velocity orthogonal to the E-M line within the E-M plane.

INTRODUCTION

This report is the first of a series intended to depict classes of orbits of the restricted problem of three bodies and to compare these orbits with orbits of the Kepler problem, the latter of which refer to a rotating coordinate system.

The purpose of these publications is twofold: Since the model of the restricted problem with suitable mass-ratio may serve as a good approximation to the Earth-Moon (E-M) model, the results will be of assistance to the mission designer concerned with the selection of E-M trajectories. In accordance with this, the terms "Earth-Moon orbits" and "orbits of the restricted three-body problem" will be used interchangeably in this report.

The second purpose is tutorial -- that of helping the scholar in acquiring familiarity with the characteristics of orbits of the restricted three-body problem, and, by the concurrent showing of comparable Kepler orbits, contributing to the understanding of many peculiarities encountered in the restricted problem.

The class of E-M orbits discussed in this report is determined by the common initial position on the axis of the masses, one half E-M distance beyond the moon and the initial velocity being orthogonal to the mass-axis, in the plane of motion of the masses. The range in which velocity variations are made is essentially that range for which the Kepler orbits are elliptical.

Since Kepler orbits, as viewed from a rotating reference system, have obtained rather limited promulgation, an introductory section on these orbits is included as part of this report.

The comparative study of the orbit classes is arranged in two sections, the first offering a synoptical viewing of orbit arrays with each orbit shown for a limited length of time, and the second section tracing and comparing single orbits over extended histories.

The appendix compiles information related to the mathematical problem description and the methods of regularization and integration as applied in the computational program that was used in the preparation of the material presented.

KEPLER ORBITS IN ROTATING COORDINATES

The model of the Kepler problem is arrived at by making the following transition from the normalized model of the restricted problem of three bodies. The smaller of the two attracting masses, i.e., the mass μ, is reduced to zero while the sum of the two masses is maintained at unity. In this process both the distance between the two attracting masses and their rate of circular revolution about their common mass-center are maintained at unity. Two Cartesian coordinate systems, the inertial (X, Y) and the rotating coordinate system (X_R, Y_R), are used in this report. The latter rotates with the masses, the X_R-axis placed through the two attracting centers and the Y_R-axis placed through the common center in the plane of their revolution. The two coordinate systems are coinciding at initial time.

After the transition from the model of the restricted three-body problem to that of the Kepler problem has been made, the origin of both systems is at the only remaining mass.

The limit point of the location of the second (vanishing) mass is at the X_R-axis at distance unity. This point may be coined the "empty mass point" and marked "L" for later reference, where its significance will be discussed. As to the orientation of orbits in the Kepler problem, the convenience of having the apses of the orbits on the abscissas of the two systems at initial time is utilized. In this way, the objective of comparing these orbits to those of the three-body problem is met most easily. For the explanations to follow, attention is drawn to the different definitions that some terms will have in the two systems of reference used here, i.e., the inertial (or space-fixed or sidereal) and the rotating (or synodic) coordinate systems. Frequent use of the identification of orbits by their mean-angular motion "n," as defined with reference to the inertial system, will be made.

The reason for this lies in the convenient interpretation this term finds in the rotating system. This will now be developed.

A condition for Kepler orbits to be periodic or returning to their initial state coordinates in finite time in the rotating reference system is the commensurability of their inertial period P_I with the period 2π of the rotating system in the inertial frame. Making use of the relationship $n = P_I/2\pi$ results in the requirement for n to be rational for orbits to be periodic in the synodic system.

If one assumes $n = k/\ell$, with k and ℓ being relatively prime integers, the following interpretation of n is obvious. During one synodic period of the orbit with characteristic $n = k/\ell$, the coordinate system rotates ℓ-times, while an orbiter moving along the given orbit revolves k-times along this orbit, with both motions understood to be in reference to the inertial frame.

The term k is signed positive or negative in agreement with the sense of motion along the orbit as seen in the inertial frame.

Since information on synodic Kepler orbits, especially their illustration, is rather sparse in the literature, this report will devote space to a systematic discussion of them. (See also Ref. 1.)

Figure 1 shows the inertial representation of a group of Kepler orbits all of which have mean angular motions of $n = 3/4$. A fixed n-value for a group of Kepler orbits means as much as a

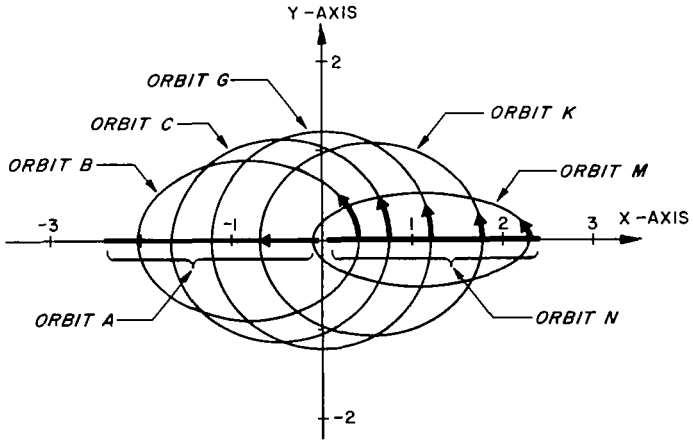

Figure 1.- Kepler orbits with n = 3/4 in inertial coordinates

fixed major axis, fixed period, and fixed energy for this group. The notion "family" is often applied to the totality of orbits of a fixed n. Note that the extremes of a family are the rectilinear flights along the X-axis between the point X = 2a and the point-mass at the origin.

The two subsequent illustrations (Figures 2 and 3) depict these orbits and several others of this family as they are viewed from the synodic coordinate system. Of the original geometric shapes there is only one retained, the circular orbit marked "G" on Figure 1. Inspecting now the series of orbits, starting at the circular one and moving in either direction, reveals a pattern development that is formed sequentially by indentations, cusps, and then loops of increasing magnitude. Each loop develops on its own an increasing indentation where it is nearest to the mass. The series terminates at both ends with orbits that show

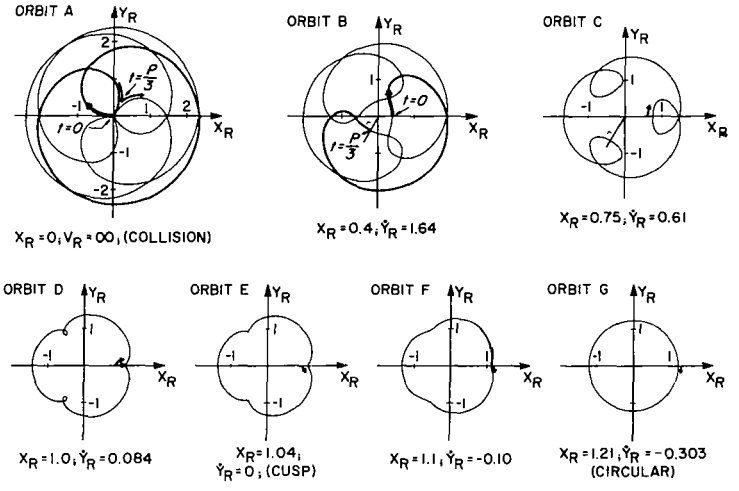

Figure 2.- Kepler orbits with n = 3/4 in rotating coordinates; Part I

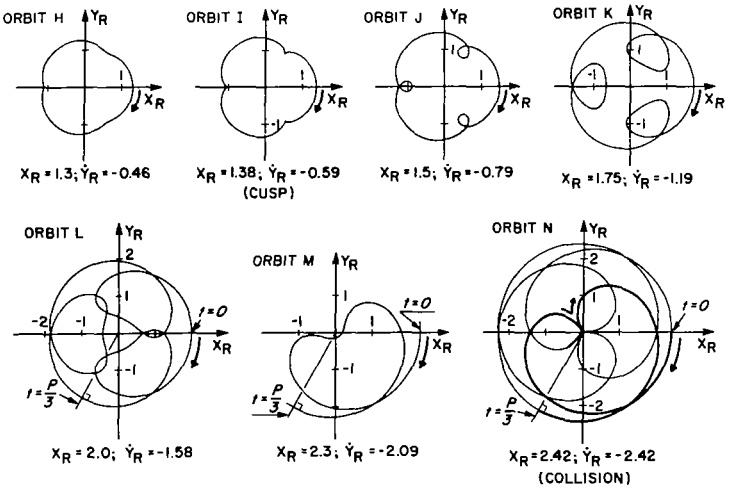

Figure 3.- Kepler orbits with n = 3/4 in rotating coordinates; Part II

a cusp-like geometry at the mass (orbits "A" and "N"). These latter cases are the collision cases, corresponding to the rectilinear cases in the inertial reference. (The term "cusp" refers to the geometry only. The infinite velocity at collision actually prohibits the use of the term here and so, subsequently, the term "cusp" will be applied only where both velocity components -- with respect to the rotating coordinate system -- vanish.)

Just as the rectilinear cases in the inertial reference can be associated to the positive-n family as well as to the negative-n family, so can the last discussed collision cases in the synodic reference be considered to terminate the positive-n family and to commence the family of the negative n-value. Synodic orbits of the negative-n family are represented on the subsequent illustrations (Figures 4 and 5). The first orbit ("0") and the last one ("X") are repetitions of orbits "N" and "A," respectively.

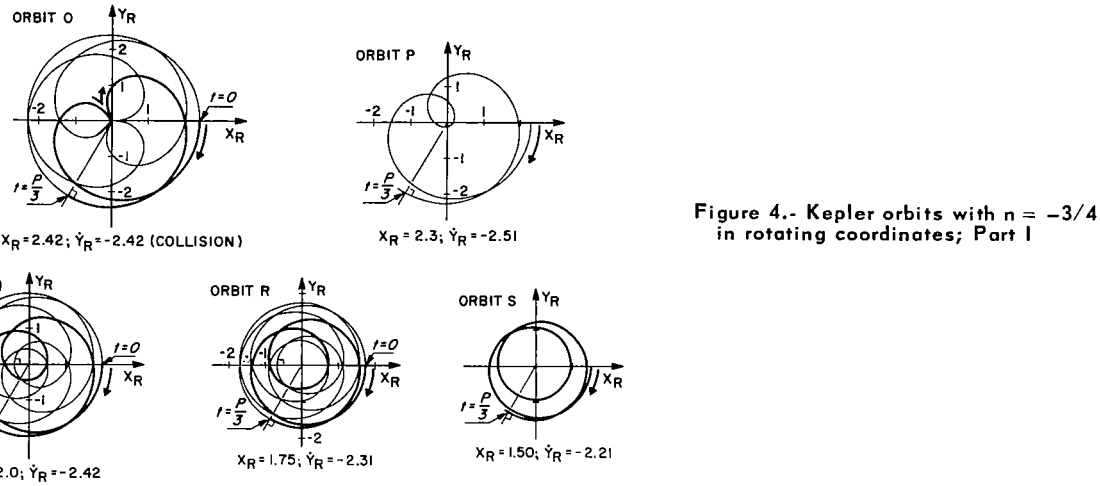

Figure 4.- Kepler orbits with n = −3/4 in rotating coordinates; Part I

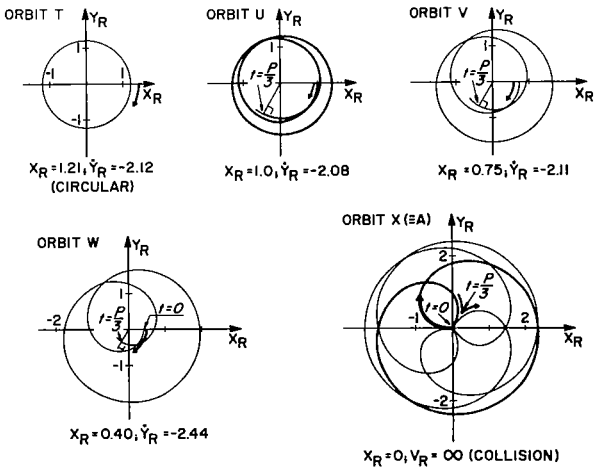

Figure 5.- Kepler orbits with n = −3/4 in rotating coordinates; Part II

Tracing the pattern development from these two extremes in direction to the center of this series, allows one to recognize that loops about the mass are formed which increase in size as the center of the series is approached. The contraction of the outer contours of the orbits which can be observed to occur with the expansion of the inner loops leads finally to the coinciding of the outer and inner traces to form a circle (orbit "T"). (Note that, for ease of reading, some of the orbits are traced for a third of the period only, the two other thirds being identical to this, but rotated by 120 and 240 degrees.) With the attainment of this circle, the full cycle, consisting of two families, is closed.

It is worth mentioning that the two circular orbits, "G" and "T," evolve from neighboring patterns that are topologically quite different from each other. While the circular orbit "G," which is of the positive family, matures through the process of contraction of loops and smoothing of dents, the orbit "T" of the negative family is formed through the convergence of a number of loops about the mass. Since here in the negative n-range, the mass center is circumscribed seven times by all orbits of the family, this circular orbit is to be run through seven times if consistency of its orbital period with that of its neighboring orbits of the family is to be maintained. The orbit G, in contrast, fits into its neighborhood if traced through only once.

To further enhance the understanding of, and familiarity with, Kepler orbits in the synodic system, five more families are depicted on the five subsequent illustrations (Figures 6-10).

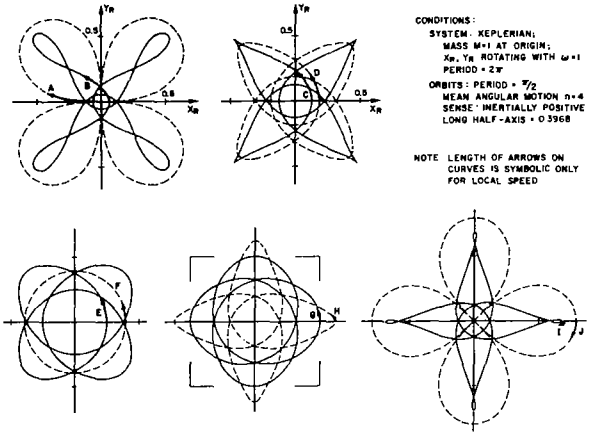

Figure 6.- Kepler orbits periodic in the rotating system: positive; n = 4

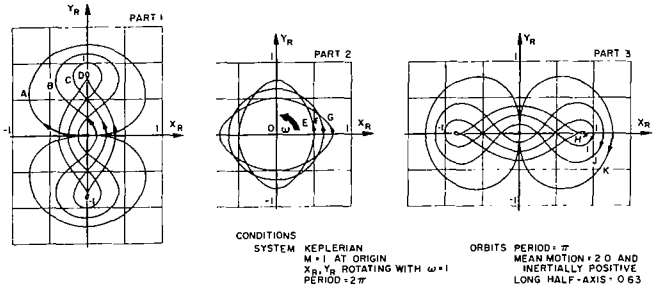

Figure 7.- Kepler orbits periodic in the rotating system: positive; n = 2

These concern the n-values 4, 2, 3/2, 4/3, and n = 1, all of positive sign only. (Note that, in most cases, several orbits have been drawn on one grid. Also, for the family n = 4/3, the limiting orbits, i.e., the collision orbits, are traced to one loop only while four of these make up the orbit.)

Characteristic for orbits of positive n-values that are larger than unity is a geometry marked by loops extending "outward" in contrast to the loops (rather lobes) of the (n < 1) cases which are directed "inward."

A case of uniqueness and, thus, of special interest is the family of n = 1, depicted on Figure 10. Since for this family the mean angular motion is the same as that of the rotating system, the orbits do not enclose the origin. Thus there also is

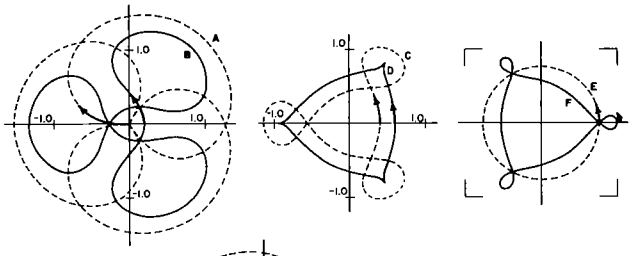

Figure 8.- Kepler orbits in the rotating system: positive; n = 3/2

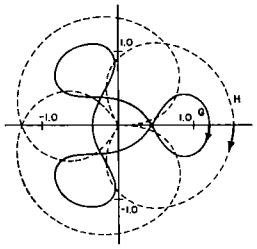

SYSTEM KEPLERIAN;
ROTATING WITH $\omega = 1.0$
ORBITS PERIOD = $2\pi/3$;
MEAN ANGULAR MOTION $n = 3/2$;
SENSE INERTIALLY POSITIVE
LONG HALF AXIS 0.7631

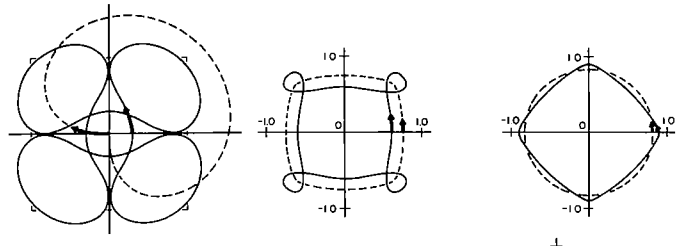

Figure 9.- Kepler orbits in the rotating system; positive; n = 4/3

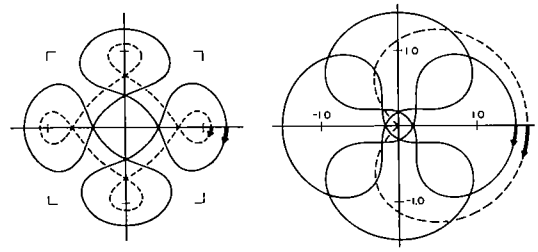

NOTE
ONLY ONE OF THE FOUR LOBES ON EITHER TERMINAL (COLLISION) ORBIT IS SHOWN.

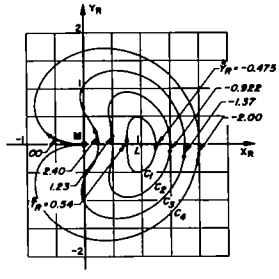

CONDITIONS:
SYSTEM: KEPLERIAN
M=1 AT ORIGIN
X_R, Y_R ROTATING WITH $\omega = 1$
PERIOD = 2π
ORBITS : PERIOD = 2π
SENSE OF REVOLVING : INERTIALLY POSITIVE, LONG HALF-AXIS a=1

Figure 10.- Libration orbits of the Kepler problem; n = 1

no circular orbit in the family. Rather the circular orbit in the inertial reference has its synodic image in a stationary point at distance unity (X_R = 1.0), i.e., the point marked "L" before. All orbits of the family envelop this point. Also, orbits of this family do not intersect one another. (For a discussion of these orbits, see ref. 2.)

Families of orbits have been discussed with respect to their internal development from member to member. An attempt will now be made to compare families with each other and thereby identify the characteristic features of families. The larger generality of statements then calls for omission of particulars which, in this case, is accomplished by selecting from each family only one representative member. The selection of each of these members is based on its capability of demonstrating the typical features of its family, as the number of loops, their structuring and sequencing, the number of times the orbit is going around the mass in a period, and so forth. Of the families, 15 have been chosen. They are shown as Figures 11-14. Again, positive-n families only are shown since the structure of negative-n families is rather easily understood. The variation of n among the illustrated cases is broad enough that the behavior of any other n-case can be found by analogy. These illustrations are evaluated in the form of a list of characteristics which follows.

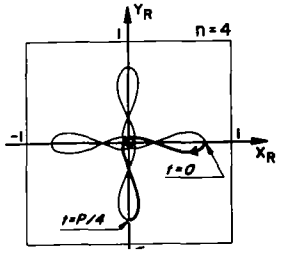

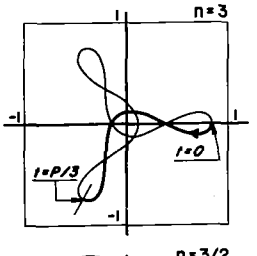

Figure 11.- Kepler orbit characterization (Part I)

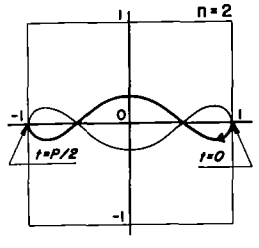

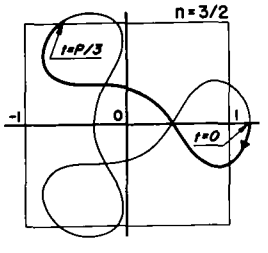

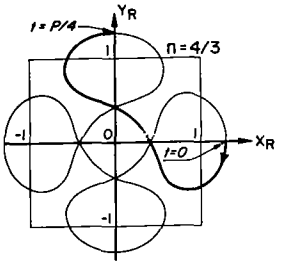

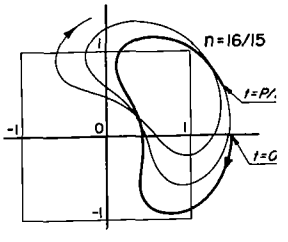

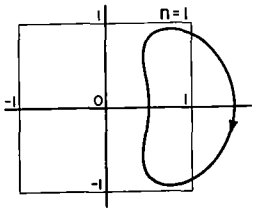

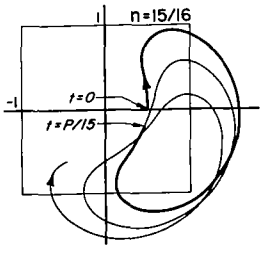

Figure 12.- Kepler orbit characterization (Part II)

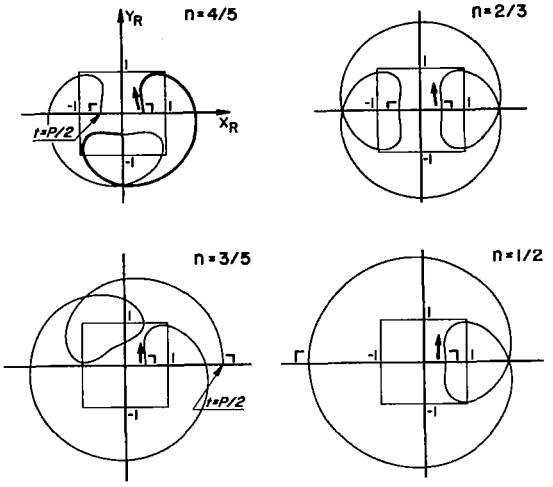

Figure 13.- Kepler orbit characterization (Part III)

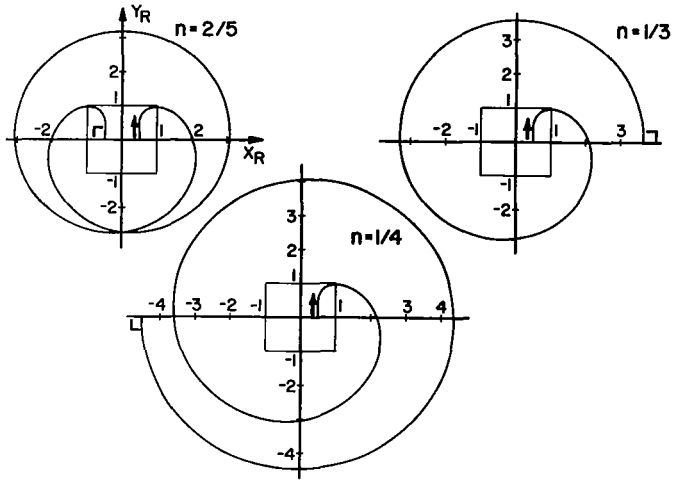

Figure 14.- Kepler orbit characterization (Part IV)

Characteristics

The following statements hold for all positive and negative n-families, except a few cases listed at the end of this section. The proof of the characteristics is foregone; the accompanying illustrations may serve to make verification and to gain understanding.

For Kepler orbits of mean angular motion $n = k/\ell$ with k and ℓ being relatively prime integers, $k \neq 0$ and $\ell > 0$, the characteristics of orbital motion, as observed in a synodic (i.e., rotating) coordinate system, are the following:

(a) The synodic period is $2\pi\ell$.

(b) The mean-angular motion with respect to the synodic reference system is $(k - \ell)/\ell$. A negative value means retrograde motion.

(c) During one synodic period an orbiter moving along the orbit goes around the mass $(k - \ell)$-times as observed in the synodic reference system.

(d) During one synodic period, the orbit develops $|k|$ identical patterns (loops, lobes, cusps, etc.)

(e) Two patterns that succeed each other in time are spaced from each other by a central angle of $2\pi(k - \ell)/|k|$.

(f) Families of negative n will not have a cusping orbit.

Qualifications are in order for the application of these rules in the following cases:

1. Circular Orbits

The synodic period according to rule (a) need not be the smallest one for circular orbits. If $|k - \ell| > 1$, an earlier period is calculated by $2\pi\ell/|k - \ell|$. However, in this case, consistency with the period of the family will not be maintained. A corresponding remark holds, of course, for rule (c).

2. Parabolic Orbits

Though parabolic orbits can be thought of as associated with $n = 0$ and will be marked correspondingly, their characteristics are found by approaching them through a sequence of small-n-families as, e.g., the sequence $1/\ell$ with ever-increasing ℓ. In this way, one finds that the period is infinite and the mean angular motion in the synodic system is negative unity. This holds for the positive as well as the negative parabolic family.

3. Libration Orbits and Libration Point L

The family of Kepler libration orbits ($n = +1$) possesses neither a circular nor cusping orbits. These are represented in degenerate form by the Kepler libration point L.

The assignment of a period to the stationary point L, according to rule (a), would only serve the purpose of preserving consistency throughout the family.

THE APSIDAL VELOCITY DIAGRAM

Since the approach to the three-body problem in the succeeding part of this report will not be in the form of a search for periodic orbits that make up a particular family, but will be rather in the form of a study of orbits that all start at a fixed origin -- and in a comparison of these orbits with Kepler orbits that also start all at one fixed origin -- a diagram which relates initial conditions to the n-value of an orbit is needed. Such a diagram will now be introduced (Figure 15).

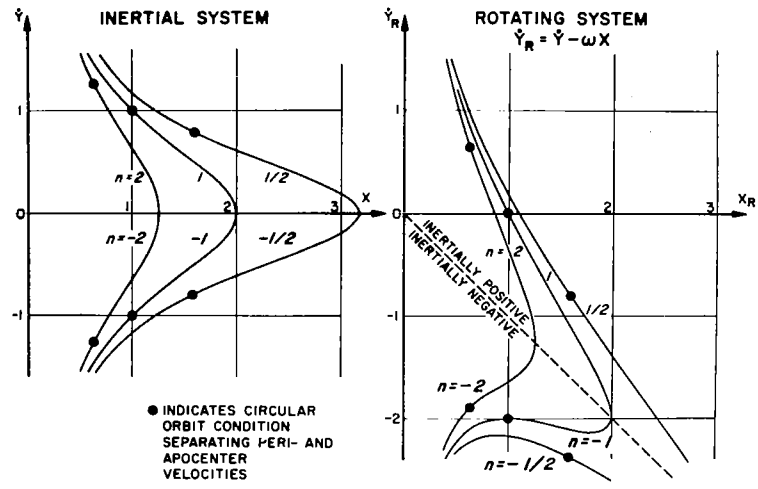

Figure 15.- Apsidal velocities in both systems for families of orbits with fixed mean motion "n" versus apsidal position on X-axis or X_R -axis

A Kepler orbit is determined by its initial conditions of position and velocity. Let the Y-value and $\dot{X}$-value be zero at initial time for all orbits under investigation. Then any orbit can be represented as a point in the system, the abscissa of which is X and the ordinate of which is $\dot{Y}$. Since $\dot{Y}$ is the velocity at the apsidal point X, the representation is called the apsidal velocity diagram. If orbits of identical mean-angular motion n are connected by lines in this diagram, the desired relationship is furnished.

Such a representation is given in the left-hand graph of Figure 15. Families of n = 2, 1, and 1/2 are shown. Since here the coordinates are inertial, the curves are symmetric with respect to the X-axis and the sign of the $\dot{Y}$-value is equal to the sign of the n-value.

If the fact is borne in mind that orbits along a constant-n curve also have constant major axis 2a, it will be recognized that the intersections of the n-curves with the X-axis give the respective rectilinear orbits, starting at 2a, colliding with the mass and returning to the initial point. Also, it will be recognized that the heavy dot marks on each curve, at an X-value halfway toward the maximum of the curve, reprsent the positive and negative circular orbits of the family.

On the right-hand graph of Figure 15 the same three n-families are shown, now plotted with respect to the rotating

coordinates X_R and $\dot{Y}_R$. Since at initial time $X = X_R$, the abscissa-values are unchanged. The ordinate-values transform according to $\dot{Y}_R = \dot{Y} - \omega X$, with ω being the angular motion of the synodic system of value unity.

Note here that now the major part of each family is initiated with negative velocity. Also all collision cases (lying on the dashed straight line) are "in the negative," and so are both circular orbits for initial positions larger than unity. Observe also that, on the lower branches of some n-curves, X_R is double-valued over some regions of $\dot{Y}_R$.

While the two graphs of Figure 15 serve primarily to introduce the concept of the apsidal velocity diagram, the diagram shown in Figure 16, by preference, will be used as the working diagram in the following discussion. Its more detailed structure shows the field of n-curves wedged in between the two zero n-curves. These limits represent all orbits of parabolic character. The highest n-value shown here is n = 2, though, of course, the field continues to the left of this curve.

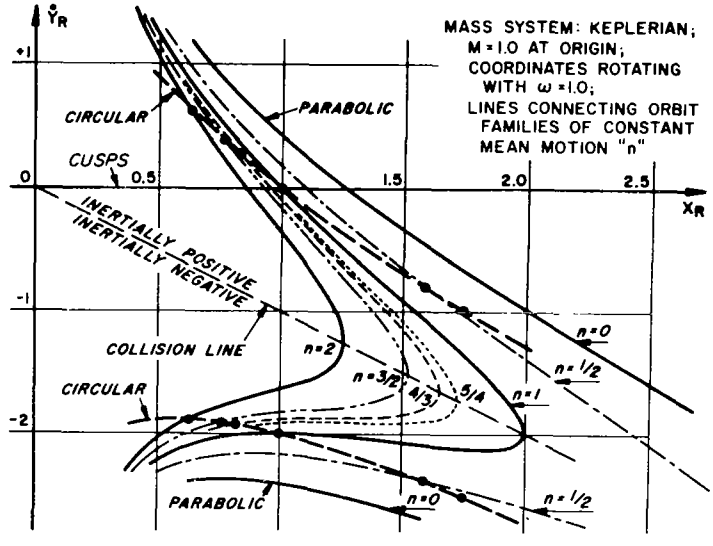

Figure 16.- Apsidal velocities in the rotating system for orbit families with fixed mean motion versus apsidal position on X_R -axis

Principal interest will be directed to the intersection of the n-field with the vertical line given by $X_R = 1.5$ since all the Kepler orbits depicted and discussed in this report will be initiated at this distance from the mass. Also, the orbits of the restricted problem of three bodies, discussed in this report, will originate at a distance of 1.5 from the heavier body.

The discussion of the Kepler series in the next section will commence with an orbit near the lower parabolic limit, will carry through the elliptical range, and terminate when orbits of small positive apsidal velocity are reached. As can be seen in this diagram, the n-families to be crossed range from n = 0 (negative) to the value near n = -3/2 whereupon the collision trajectory will be hit. Subsequently the n-values are positive and reverse in order from n = +3/2 down to n = 0 (positive). In the series, two circular families (dashed curve) will be crossed and two orbits with cusps -- one of which will be the orbit with zero initial velocity -- will be found.

While this apsidal velocity diagram will serve as a guide for the Kepler orbits as the study progresses, so the Kepler orbit series as a whole will serve as an approximation to the series of three-body orbits started at a corresponding initial point. Both series will be discussed simultaneously.

COMPARATIVE GRAPHICAL DESCRIPTION OF A SERIES OF ORBITS OF THE RESTRICTED PROBLEM OF THREE BODIES AND A SERIES OF KEPLER ORBITS IN ROTATING COORDINATES

Preparatory Remarks

The model of the restricted problem of three bodies, as employed here, is that of two point-masses ($1 - \mu$ and μ), at unity distance from each other, revolving with unity angular motion ω about their common mass center. The mass parameter μ is chosen as 1/80. A rotating Cartesian coordinate system X_R and Y_R is defined such that the origin is at the mass center and the masses on the abscissa at $X_R = -0.0125$ and $+0.9875$ for the larger and smaller masses, respectively. For convenience, the masses will be referred to frequently as Earth and Moon, or E-M.

The objective of this report is to bring into comparison a series of orbits of the restricted three-body problem with a series of Kepler orbits. The three-body series is defined by the initial conditions

$$X_R = 1.4875; \qquad Y_R = 0; \qquad \dot{X}_R = 0; \qquad \dot{Y}_R \text{ varied},$$

the differentiation being understood with respect to the normalized time variable. The Kepler series collated to this series is defined by $X_R = 1.5000$; $Y_R = 0$; $\dot{X}_R = 0$; $\dot{Y}_R$ varied. The initial points are chosen such that their distances to the heavy mass (or only mass, in the Kepler case) are identical in the two series.

There is no fixed time length for which orbits are studied; rather the time is dictated by the case history itself. On the average, however, the time length lies between 2π and 4π, i.e., the time of one and two lunar revolutions about the Earth.

It will not be a matter of primary concern in this study to search out periodic orbits. However, in most cases where, in the course of progression, cases of periodic orbits are encountered, they are isolated and illustratively documented. In other cases, it was considered satisfactory to point out the existence of periodic cases by showing sequences of orbits that clearly are positioned at both sides of a periodic orbit. Where a periodic orbit is pictured, it is usually traced to its first orthogonal crossing of the X_R-axis. This crossing of the axis is at half the orbit's period, the second, reflected half of the orbit being omitted in the interest of greater clarity.

The comparison of the two series will be made twice. The first time, an overall view of the orbit series of one problem will be set in correspondence to an overall view of the counter-series. This view will be concerned with short time histories of the orbits only and therefore will allow the composite exposition of a fair number of orbits on a single graph.

In the second comparison, individual orbits of the restricted problem will be depicted one by one, in a sequence that will be dense enough to relate pictorially all events of relevance as far as they occur in the time interval of 4π after the initial time. These will then be set into relation to Kepler orbits as they fit best.

Subsequently, the three-body orbits will be consistently shown at the upper half of the page and the Kepler orbits on the lower half of the page.

Comparison of Short-Term Synopses

The near-time behavior of the orbits of the restricted three body problem, starting at $X_R = 1.4875$ in axis-orthogonal direction, is aptly characterized in Figures 17, 19, and 21. Their Kepler counterparts are shown as Figures 18, 20, and 22.

The upper series (Figure 17) is started with the orbit of initial velocity $\dot{Y}_R = -2.47$, a value not far from the escape cases which would be represented by orbits spiralling out to infinity. Initial velocities on this first graph are increasing to a value of $\dot{Y}_R = -1.5$, associated to the innermost orbit. Intersections of the orbits with the X_R-axis move successively closer to the Earth. The last orbit of this group is an Earth-collision orbit.

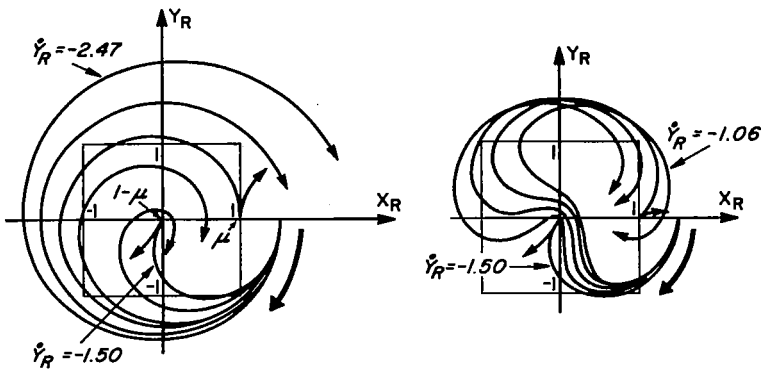

PART I : INITIAL VELOCITIES $\dot{Y}_R$ BETWEEN -2.47 AND -1.50

PART II : INITIAL VELOCITIES $\dot{Y}_R$ BETWEEN -1.50 AND -1.06

Figure 17.- Earth-Moon field: orbit synopsis, Part I and II

The next group of Figure 17, which repeats the last collision orbit and shows orbits of initial velocities up to $\dot{Y}_R = -1.06$, demonstrates how the orbits "squeeze-in" between the two masses to intersect the X_R-axis. The second intersection of the orbits with the X_R-axis, however, moves further out toward the point where the orbits start. Studying then the corresponding graphs of Figure 18, one observes a close similarity of the Kepler orbits with those of the three-body problem.

The obvious difference of behavior develops when orbits of the upper series collide with the Moon, which event occurs once in each of the two groups. It will be shown in the next section, that there is a neighborhood of orbits to these collision orbits that will show the influence of the moon on their flight course.

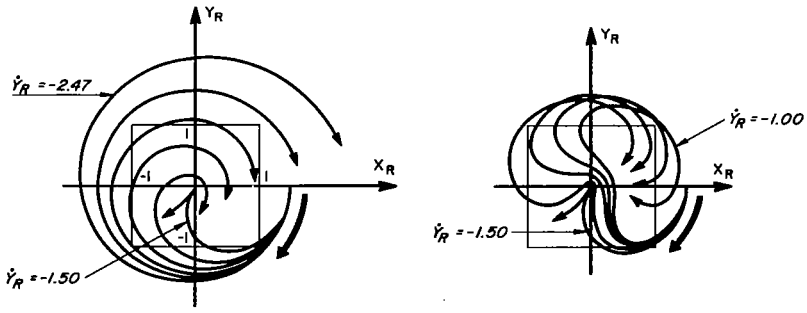

PART I: INITIAL VELOCITIES $\dot{Y}_R$ BETWEEN -2.47 AND -1.50

PART II: INITIAL VELOCITIES $\dot{Y}_R$ BETWEEN -1.50 AND -1.00

Figure 18.- Central force field: orbit synopsis, Part I and II

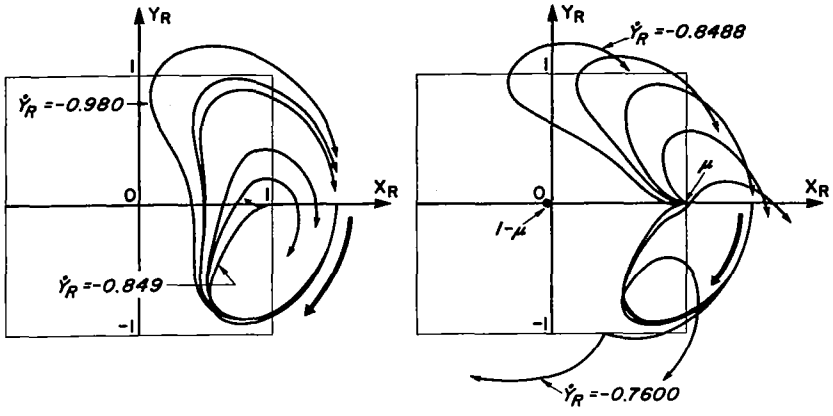

PART III : INITIAL VELOCITIES $\dot{Y}_R$ BETWEEN -0.980 AND -0.849

PART IV : INITIAL VELOCITIES $\dot{Y}_R$ BETWEEN -0.8488 AND -0.7600

Figure 19.- Earth-Moon field: orbit synopsis, Part III and IV

Progressing now to Figure 19, it can be seen that from orbit to orbit the loops around the Moon contract to a smaller size until lunar impact is encountered with the initial velocity of -0.849. The orbits that follow this collision orbit in the sequence of the series, as shown in the second graph of Figure 19, circumnavigate the Moon in a direction opposite to that flown by the orbits on the left-hand graph; after a larger "excursion" into the region ahead of the Moon, they return to the original direction of mean angular motion. With increasing initial velocity, the loops of the orbits shrink and finally degenerate into a cusp.

If there is interest in large-scale characterization of the orbits, e.g., a characterization of entire groups among each other, the two groups of Figure 19 are both concerned with "near-Moon" orbits, while this characterization is not applicable to the two first groups discussed. As will be seen in the next section, the "near-Moon" groups have among their orbits a number of periodic ones that stay permanently in the neighborhood of the Moon.

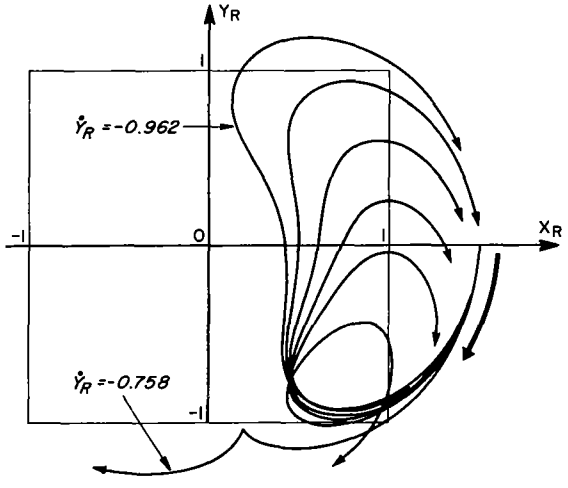

INITIAL VELOCITIES $\dot{Y}_R$ BETWEEN -0.962 AND -0.758

Figure 20.- Central force field: orbit synopsis, Part III

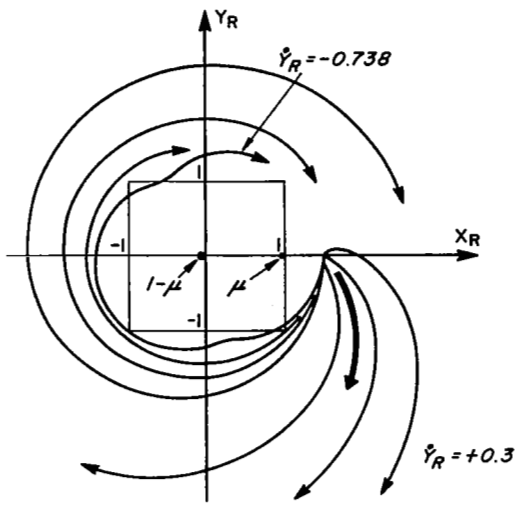

PART V: INITIAL VELOCITIES $\dot{Y}_R$ BETWEEN 0.738 AND +0.30

Figure 21.- Earth-Moon field: orbit synopsis, (concluded)

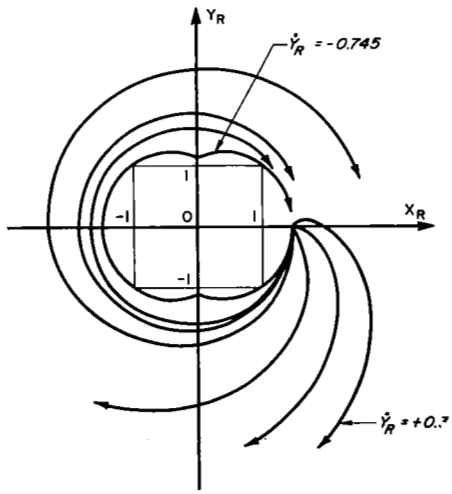

INITIAL VELOCITIES $\dot{Y}_R$ BETWEEN -0.738 AND +0.30

Figure 22.- Central force field: orbit synopsis, Part IV (concluded)

The group of Kepler orbits that forms the counterpart to the "near-Moon"-groups of the three-body problem is depicted in Figure 20. The development is rather clear-cut, with loops decreasing in size and simultaneously moving in retrograde direction. At the end of this development, there is again the orbit with cusps, with nearly the same initial velocity (-0.758) as was used for generating the cusping orbit of the three-body series. The Kepler series development is simpler than that of the three-body series since the disturbance by the Moon is absent.

Figure 21 then depicts the terminal phase of the orbit development of the Earth-Moon field. The group starts at the innermost orbit, which lies in the development near to the cusping orbit of the former group. With the initial velocity increasing, the orbits assume patterns that enlarge radially from one orbit to the next. The general development, one notices, is the reverse of that of the very first group of the sequence (i.e., that of Figure 17), which means that finally orbits are obtained which are spiralling outward at a rate that grows with the initial velocity. The last orbit shown (with $\dot{Y}_R = +0.3$) is well in the range of escaping orbits. As Figure 22 shows, this development is not different from that of the Kepler series.

Comparison of Individual Orbits over Longer Periods

Both series will now be considered once more, this time in a denser orbit progression and with attention to longer orbital histories.

The density of selection of orbits in the Kepler series will be dictated by the objective of presenting a coherent development of the family-structure in the same sense as mentioned in an earlier part of this report.

For the series of the restricted problem of three bodies, the choice of the advances in the orbit-to-orbit progression will be guided by the desire of recording all interesting events generated in the series within the time period each orbit is followed.

Events of the restricted problem that serve to corroborate the comparativeness of orbits of the two problems studied are the occurrences of periodic orbits that can be identified as counterparts of Kepler orbits. These three-body orbits will be assigned an identification in terms of n*-values that are identical to the values characterizing the referenced Kepler orbit. The n*-value, of course, will not have the physical meaning of relating the mean angular motion as the n-value has, though in most cases it may be taken as a fairly good approximation.

However, the series of the restricted problem exhibits many interesting events that are peculiar to itself and are not to be found in the Kepler series. This is responsible for a large number of orbit drawings to be shown for which no Kepler orbit counterparts are furnished.

For deciding on an appropriate starting point in the series, knowledge of practical identity of the two series in the hyperbolic range precluded showing orbits in this range. In fact, this practical identity is preserved for orbits in the elliptical range, if they are still close enough to the parabolic boundary.

Thus, this area provides a natural starting point. The first three orbit pairs depicted (Figures 23-28) demonstrate the fact of near-identical behavior in the two series. The n-values

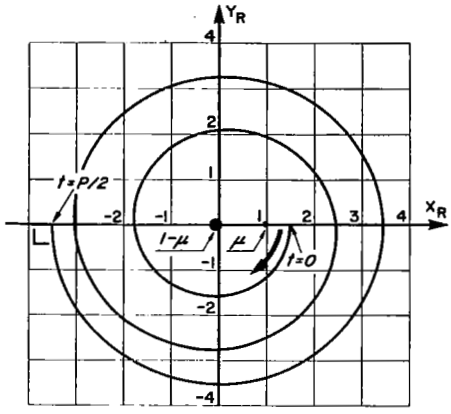

n*=-1/4
$\dot{Y}_R$=-2.4657
P/2=12.55

Figure 23

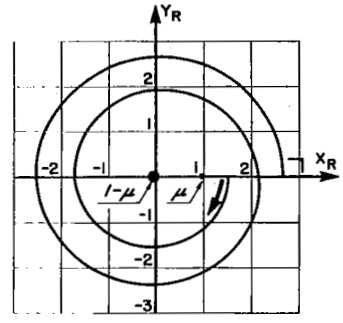

n*=-1/3
$\dot{Y}_R$=-2.4215
P/2=9.41

Figure 24

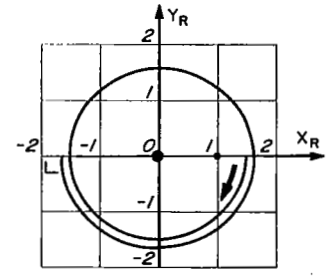

n* = -1/2
$\dot{Y}_R$ = -2.3363
P/2 = 6.25

Figure 25

ORBITS START AT X_R = 1.4875

are -1/4, -1/3, and -1/2, and correspondingly the n*-values. From these examples it is also clear what shape and topology the orbits of smaller (absolute) n-values will have (as -1/5, -1/6, etc.) approaching ever closer the parabolic orbit.

The fourth orbit pair illustrated (Figures 29, 32) is that of a circular orbit in the Kepler series and its near-circular counterpart in the upper series.

Subsequently, a first example of orbits is shown where the Kepler orbit cannot be paired to a periodic orbit of the

KEPLER ORBITS IN ROTATING COORDINATES

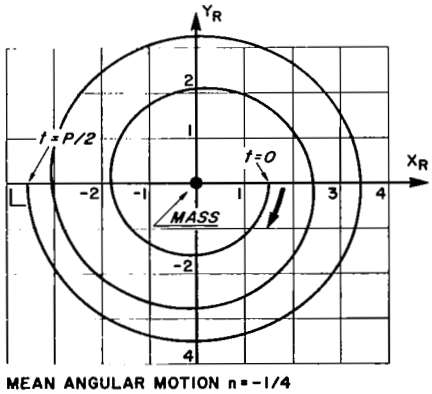

MEAN ANGULAR MOTION n=-1/4
INITIAL VELOCITY $\dot{Y}_R$ =-2.4677
HALF-PERIOD P/2=12.57

Figure 26

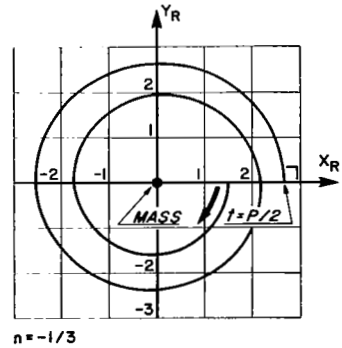

n=-1/3
$\dot{Y}_R$=-2.4234
P/2=9.42

Figure 27

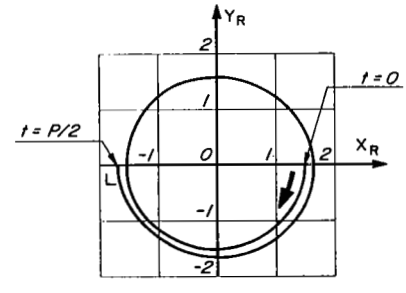

n = -1/2
$\dot{Y}_R$ = -2.3386
P/2 = 6.28

Figure 28

ORBITS START AT X_R = 1.50

EARTH-MOON FIELD ORBITS

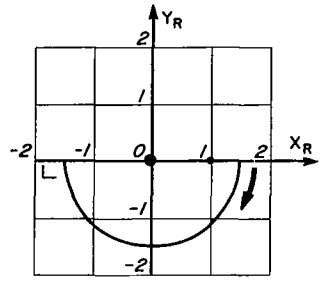

(CIRCLE - COORDINATED)
$\dot{Y}_R$ = -2.3138
P/2 = 2.02

Figure 29

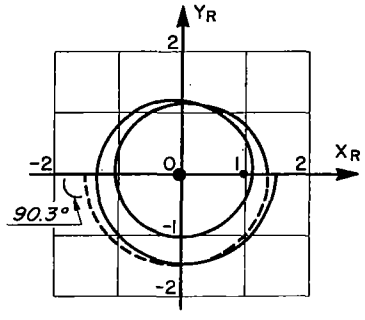

(BEST APPROACH TO PERIODIC)
$\dot{Y}_R$ = -2.2455
REF. TIME : 9.21

Figure 30

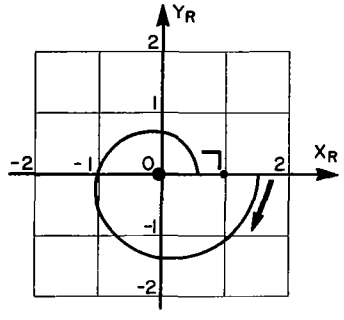

n* = -1
$\dot{Y}_R$ = -2.1005
P/2 = 3.21

Figure 31

top series (Figures 30 and 33). The best orbit in the three-body series to match the Kepler orbit of n = -2/3 is that shown for $\dot{Y}_R$ = -2.2455, which at the comparable axis-crossing fails by 0.3 degree of reaching orthogonality.

The lack of agreement of this orbit with the Kepler orbit of n = -2/3 is explainable by the nearness at which this orbit passes at its second X_R-axis crossing by the Moon--located at X_R = 0.9875. In contrast to this, the next E-M orbit (i.e., that for n* = -1 on Figure 31) has its second X_R-axis crossing sufficiently away from the masses that its behavior is quite similar to its Kepler counterpart (Figure 34).

The fact that the two orbits on Figures 30 and 31 pass by the Moon on opposite sides when they cross the X_R-axis the

KEPLER ORBITS

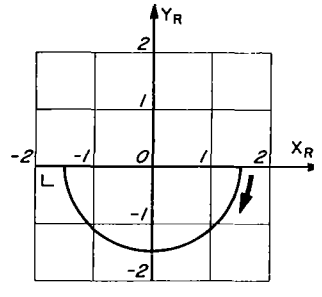

CIRCULAR ORBIT (NEGATIVE)
$\dot{Y}_R$ = -2.3165
P/2 = 2.03

Figure 32

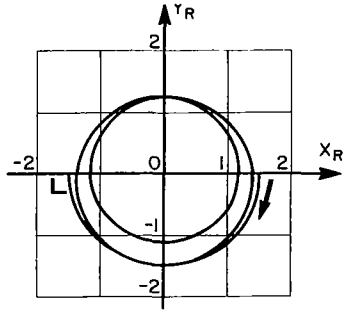

n = -2/3
$\dot{Y}_R$ = -2.2551
P/2 = 9.42

Figure 33

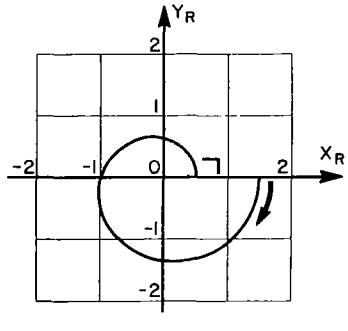

n = -1
$\dot{Y}_R$ = -2.0773
P/2 = 3.14

Figure 34

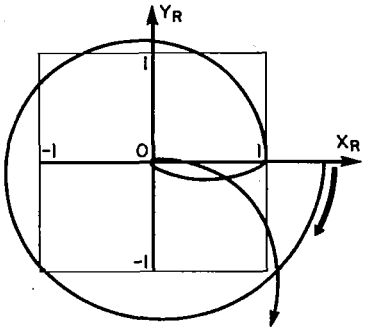

REFERENCE ORBIT
$\dot{Y}_R$ =-2.22020
FLY BY TIME (MOON): 3.720
FLY BY TIME (EARTH): 4.132

Figure 35

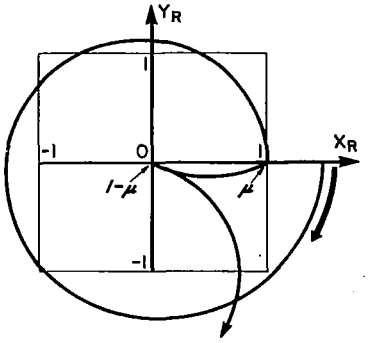

COLLISION ORBIT
$\dot{Y}_R$ =-2.22012
FLY BY TIME (MOON): 3.720
COLLISION TIME (EARTH): 4.119

Figure 36

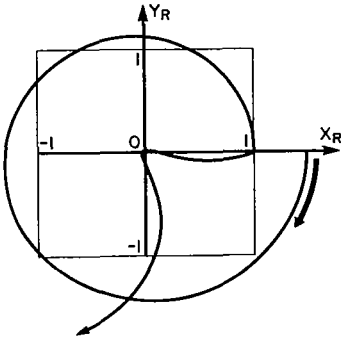

REFERENCE ORBIT
$\dot{Y}_R$ =-2.2200
FLY BY TIME (MOON): 3.719
FLY BY TIME (EARTH): 4.111

Figure 37

second time points to the existence of a lunar collision for an orbit with intermediate initial velocity. In an attempt to isolate this occurrence, one comes across the interesting case of two collision orbits being close together, one colliding with the Earth, the other colliding with the Moon. These events are delineated in a sequence of six orbits in Figures 35-40. For the first three of the orbits (Figures 35-37), attention is drawn mainly to the orbit behavior near Earth. The classical sequence of events near a collision orbit is developed insofar as the second orbit in the group depicts the exact collision, while the first and third orbits show close flyby orbits in directions around the Earth opposite to each other. For the mean angular motion "in the large," however, it is worth noting that

EARTH-MOON FIELD ORBITS

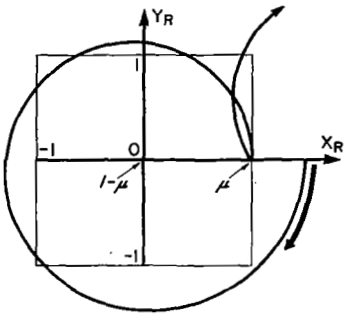

REFERENCE ORBIT
$\dot{Y}_R = -2.2192$
FLY BY TIME (MOON): 3.715

Figure 38

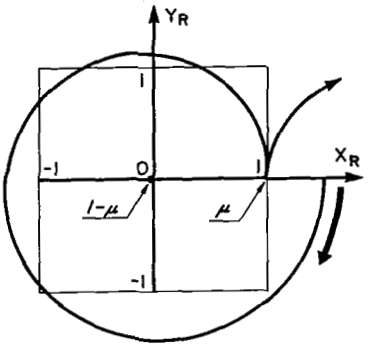

COLLISION ORBIT (MOON)
$\dot{Y}_R = -2.2190$
COLLISION TIME: 3.715

Figure 39

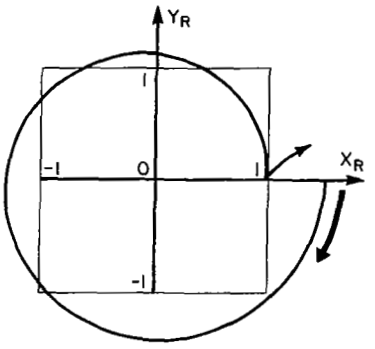

REFERENCE ORBIT
$\dot{Y}_R = -2.2188$
FLY BY TIME (MOON): 3.714

Figure 40

all orbits finally again assume the retrograde motion which they originally followed.

While for the three orbits shown in Figures 35-37, the motion around the Moon shows little change, the three orbits shown in Figures 38-40 then develop the events connected with the lunar collision. The orbit shown in Figure 39 represents the exact collision with the Moon. It is flanked by close flyby orbits, doubling the lunar mass point in directions opposite to each other, as seen by an observer on the Moon. Again, after leaving the neighborhood of the mass, all orbits assume the retrograde sense of mean angular motion, which they originally followed. It is of interest to observe that all six orbits are initiated by velocities that lie in a space of $\Delta\dot{Y}_R = 0.0014$.

At this point, Figure 41, which is an annotated version of the apsidal-velocity diagram (Figure 16, page 12), will serve to orient the reader as to the current position in the series. On this figure, the range that has been covered up to this moment is marked by the lower bracket.

The bracket above it embraces the range in the series that will be entered shortly. As seen on this diagram, the series enters the range of its highest n-values.

The peak is reached with $\dot{Y}_R = -1.5$ which is the (only) Kepler collision orbit of this series. Past this orbit in the development, the mean angular motion, which reaches a value of slightly more than $|n| = 3/2$, reverses its sign and falls off in value.

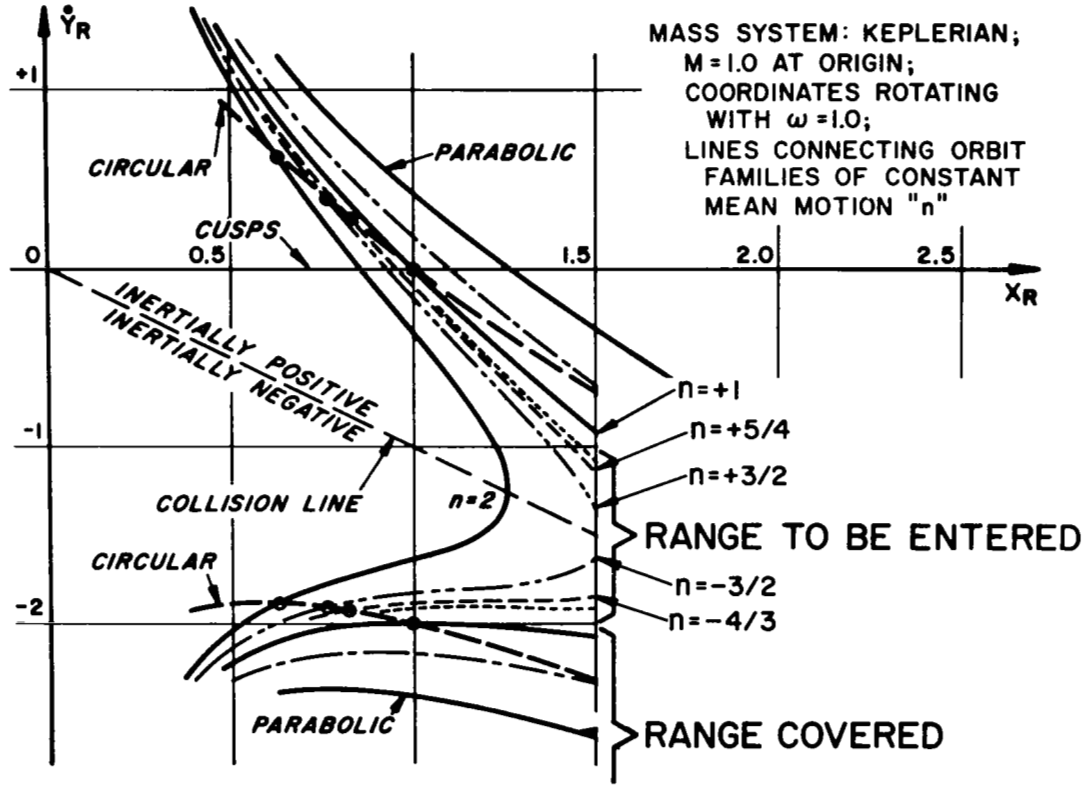

Figure 41.- Apsidal velocities in the rotating system for orbit families with fixed mean motion

Figures 42 through 53 depict orbits falling into the n-range from -4/3 to +4/3, with the three-body orbits (top of page) closely resembling the Kepler orbits (bottom of page).

EARTH-MOON FIELD ORBITS

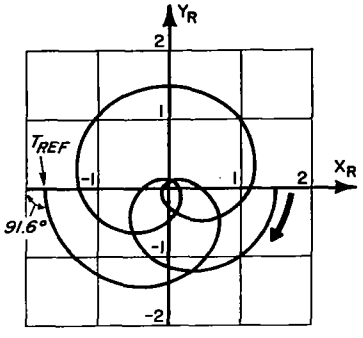

BEST APPROACH TO PERIODIC
$\dot{Y}_R$ = -1.810
T_{REF} = 9.46

Figure 42

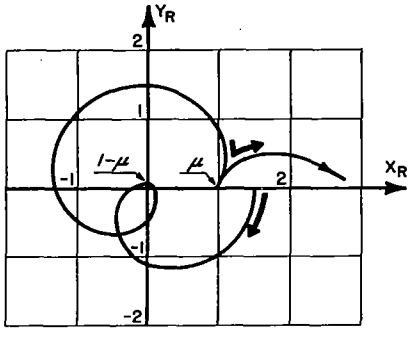

COLLISION WITH MOON
$\dot{Y}_R$ = -1.750
COLLISION TIME: 5.97

Figure 43

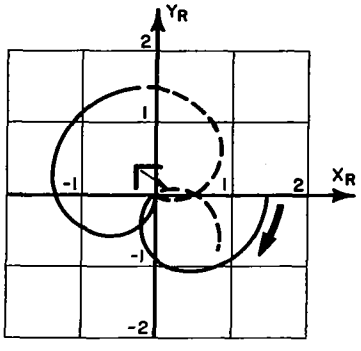

n* = -3/2
$\dot{Y}_R$ = -1.568
P/2 = 6.30
DASHED LOBE CUTS X_R-AXIS AT 90°

Figure 44

In particular, the first and third Kepler orbits (Figures 45 and 47) show the n-values of -4/3 and -3/2. The orbits on Figures 52 and 53 have the same n-values, but of positive sign and in reversed order. The orbit on Figure 51 is the collision orbit, with its initial velocity value identical, but negative, to its position value. The second orbit of this group (i.e., Figure 46) is provided here for reason of comparison with its counterpart of the three-body series.

The orbits of the three-body problem, which are arranged (Figures 42, 43, 44, 48, 49, and 50) appropriately above the corresponding Kepler orbits, reflect approximately the development

KEPLER ORBITS

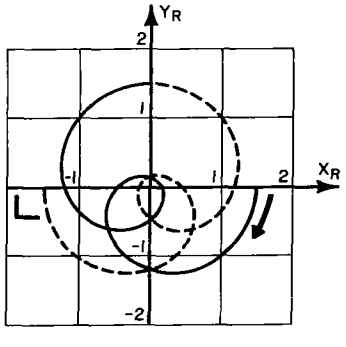

n = -4/3
$\dot{Y}_R$ = -1.849
P/2 = 9.42

Figure 45

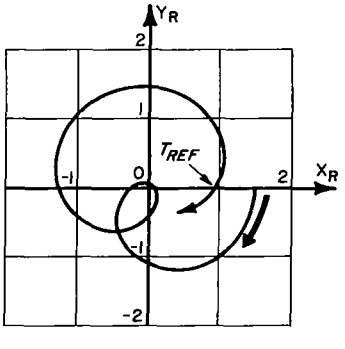

(REFERENCE ORBIT)
$\dot{Y}_R$ = -1.750
T_{REF} = 5.94

Figure 46

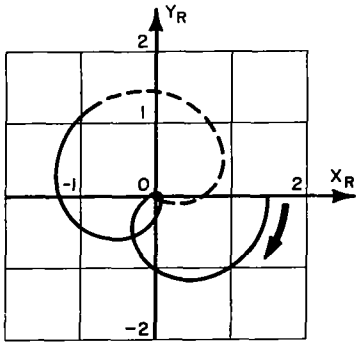

n = -3/2
$\dot{Y}_R$ = -1.652
P/2 = 6.28
DASHED SEGMENT CUTS X_R-AXIS AT 90°

Figure 47

EARTH-MOON FIELD ORBITS

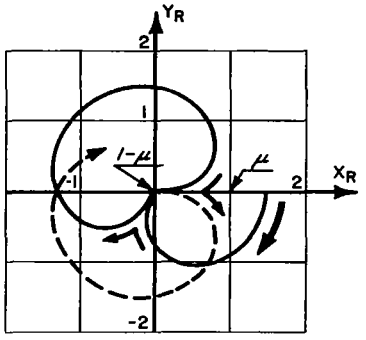

$n^* = \pm 3/2$
$\dot{Y}_R = -1.500$
COLLISION TIMES: 2.0; 6.3; 10.6; ETC.
PERIODIC COLLISION WITH EARTH

Figure 48

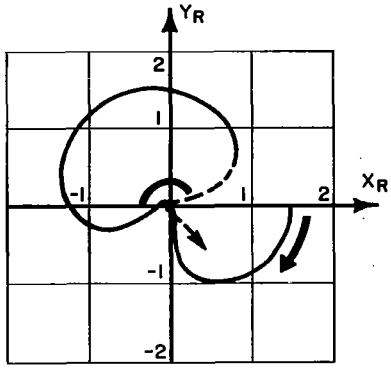

REFERENCE - ORBIT
$\dot{Y}_R = -1.35$
$T_{Ref} = 6.54$ (ON X_R -AXIS)
REF. ANGLE: 97°

Figure 49

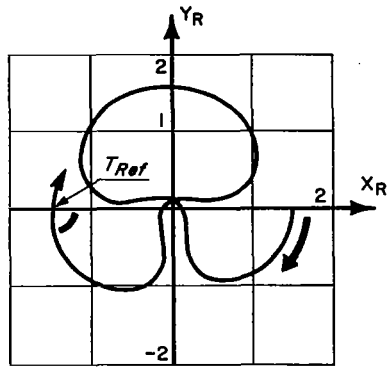

BEST APPROACH TO PERIODIC
$\dot{Y}_R = -1.21$
$T_{Ref} = 9.52$
REF. ANGLE: 85.7°

Figure 50

of the Kepler orbits. The first of the group is a "best match" to the Kepler orbit of n = -4/3, while the third is periodic and fits well the structure of its Kepler partner. Again, "best match" is all that could be found to compare with the last Kepler orbits of n = +4/3. The three-body counterpart to the Kepler collision case, however, is a fine example of a periodic collision orbit, with initial velocity not different from that of the Kepler orbit. Its periodicity characteristic is $n^* = +3/2$; thus, this orbit combines the characteristics of two of the opposite series. Of the remaining two orbits of the upper group, the orbit (with $\dot{Y}_R = -1.35$) following the collision orbit only serves the purpose of suggesting the mode of transition between its neighbors. The

KEPLER ORBITS

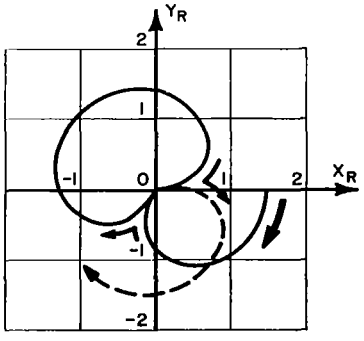

COLLISION
$\dot{Y}_R = -1.500$
COLLISION TIMES: 2.04; 6.12; ETC.

Figure 51

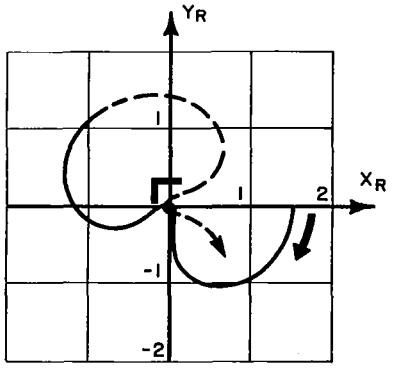

n = +3/2
$\dot{Y}_R = -1.348$
P/2 = 6.28

Figure 52

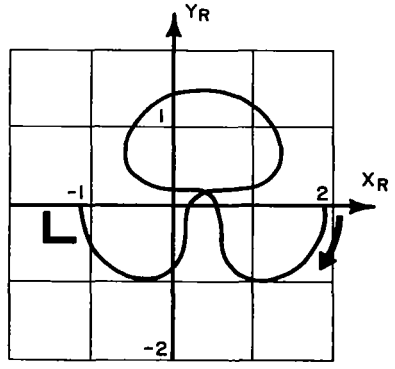

n = +4/3
$\dot{Y}_R = -1.151$
P/2 = 9.42

Figure 53

EARTH-MOON FIELD ORBITS

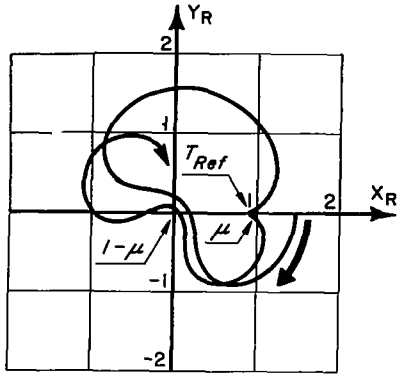

REFERENCE ORBIT

$\dot{Y}_R$ = -1.130

T_{Ref} = 6.80

Figure 54

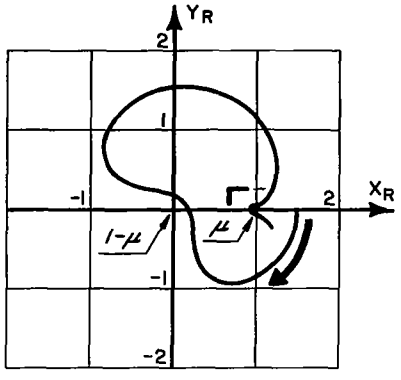

PERIODIC ORBIT

$\dot{Y}_R$ = -1.12884

P/2 = 6.80

Figure 55

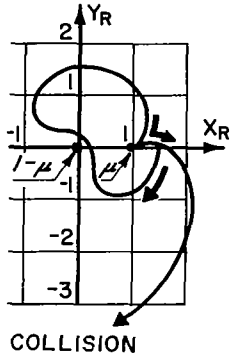

COLLISION WITH MOON

$\dot{Y}_R$ = -1.1260

COLL. TIME: 6.80

Figure 56

earlier orbit, however, with $\dot{Y}_R$ = -1.750, exhibits another mode of colliding with the Moon. Its neighboring orbits were not explored further, though it is obvious that, to its left, before the velocity reaches $\dot{Y}_R$ = -1.810, there is again a case of collision with the Earth.

Figures 54-58 represent five orbits of the restricted problem. They may be loosely identified as being in the transition area between general orbits and lunar satellite orbits. "General orbits," in this connotation, can be defined as orbits that have a non-zero mean angular motion with respect to the heavier mass as reference point, and lunar satellite orbits are orbits of zero angular motion with respect to the heavier mass, but non-zero angular motion with respect to the smaller mass as reference point, with all motion observed in the rotating system.

This group of five orbits (Figures 54-58) shows that there is no sharp dividing line between these two classes. The second and fifth orbits of the group are lunar satellite orbits, while the fourth is meeting the characterization of a general orbit. All three are periodic and therefore known in their full courses. The very first of this group is not identified in this respect; its showing serves the purpose of giving aid in recognizing the transition between its neighbors. The reason for including the middle orbit of the group (with $\dot{Y}_R$ = -1.1260) is obvious, viz., that this is another collision orbit with the Moon.

The two Kepler orbits shown in Figures 59 and 60 illustrate the trend that is characteristic for the current velocity level;

EARTH-MOON FIELD ORBITS

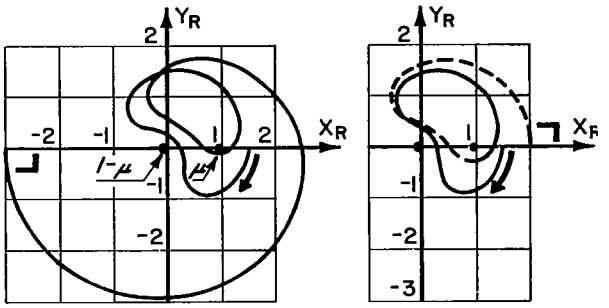

PERIODIC ORBIT
$\dot{Y}_R$ = -1.0997
P/2 = 14.95

Figure 57

PERIODIC ORBIT
$\dot{Y}_R$ = -1.0604
P/2 = 12.21

Figure 58

i.e., that the angular spacing between successive loops decreases with progression in the series. This fact supports materially the formation of lunar satellite orbits in the restricted problem of three bodies.

The region of lunar satellite orbits is the subject of interest for the next six orbits shown in Figures 61-64, 67, 68. First, however, the development that is in progress in the comparable region of the Kepler series may be studied. This development is represented in Figures 65, 66, 69, and 70. The decrease in angular spacing of successive loops, observed on the former diagram of the Kepler series, has progressed further with the

KEPLER ORBITS

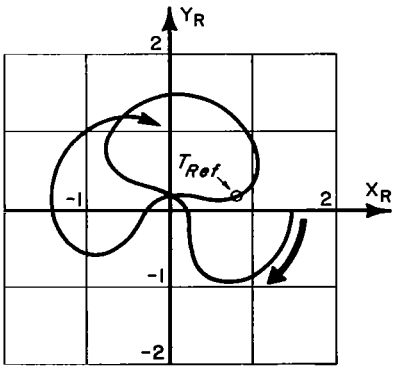

REFERENCE ORBIT
$\dot{Y}_R$ = -1.100
T_{Ref} = 6.80

Figure 59

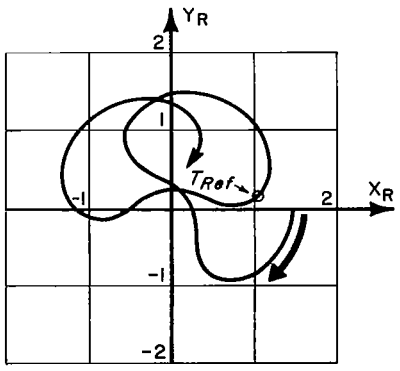

REFERENCE ORBIT
$\dot{Y}_R$ = -1.060
T_{Ref} = 6.80

Figure 60

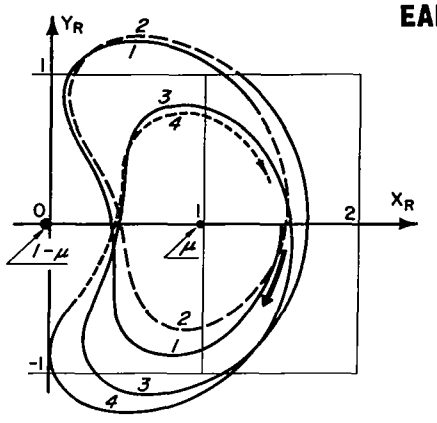

$\dot{Y}_R$ =-0.980

LOBE-HALF TIME (MEAN):3.03

(PERIODICITY NOT ESTABLISHED)

Figure 61

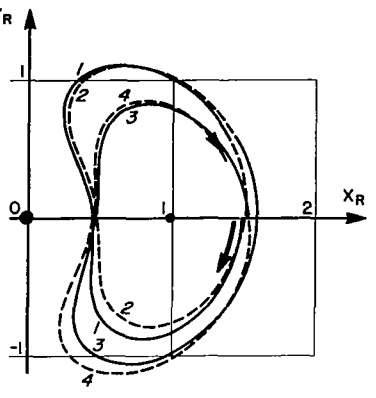

$\dot{Y}_R$ =-0.960

(PERIODICITY NOT ESTABLISHED)

Figure 62

orbit in Figure 65. The n-value here is +16/15, which indicates that there are 16 loops in the orbit. An infinite number of orbits of n-values constructed as ratios p/(p - 1) with increasing integers p will approach a limiting orbit whose n-value is unity. A comparison of this limiting orbit, however, with the orbit of n = 1 that is plotted in Figure 66, must register discrepancies in geometry as well as orbital period. A more appropriate embedding of the pictured single-loop orbit into its neighboring orbits would perhaps be obtained if in each of the neighboring orbits just one loop would be considered. Continuity in shape as well as in time-spent would prevail, but, of course, periodicity does not exist for these neighboring loops.

The single-loop Kepler orbit of n = 1 in Figure 66 is interesting for various reasons. It belongs to the family of orbits all of which include the point $X_R = 1$ and $Y_R = 0$ and they do not intersect each other. Their mean angular motion with respect to the mass, when taken in the rotating system, is zero. Orbits of this family have the character of libration orbits, with the point $X_R = 1$ and $Y_R = 0$ understood as the libration point of the Kepler system in the normalized rotating coordinate system. (Of course, any point at unity radius does as well.)

The correspondence between Kepler orbits and three-body orbits in the current energy region is rather weak. A remarkably good case of comparability, however, is found in the pair of orbits that consists of the Kepler libration orbit and its match in the upper series, shown on Figure 64. This latter orbit reproduces the geometry, velocity, and orbital period of its Kepler counterpart rather well. The similarity between them raises the

EARTH-MOON FIELD ORBITS

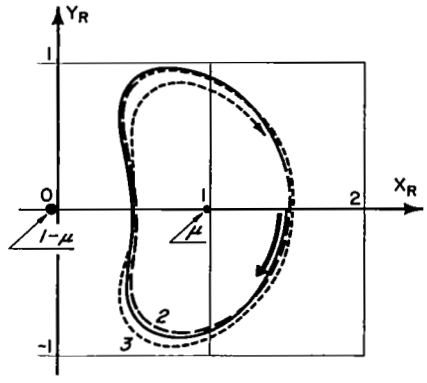

$\dot{Y}_R$ =-0.940

LOBE-HALF TIME (MEAN):3.00

(PERIODICITY NOT ESTABLISHED)

Figure 63

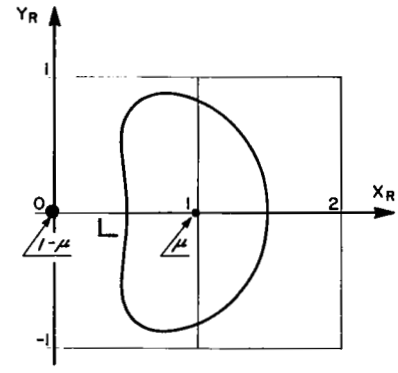

n* =+1

$\dot{Y}_R$ =-0.930243

P/2 = 2.973

Figure 64

vexing dilemma of association. This orbit is considered to be a lunar satellite orbit since it meets the definition, but it is recognized that it owes its main characteristics to the gravity field of the Earth.

The Kepler orbits depicted in Figures 69 and 70 reveal that the trend in the orbital progression reverses now, manifested in the increase of loop spacing from orbit to orbit. Also, loops are now falling behind, over time, instead of moving ahead, as observed before. Thirdly, while loops before were connected to each other at the "inner envelope," now the loops are beginning

KEPLER ORBITS

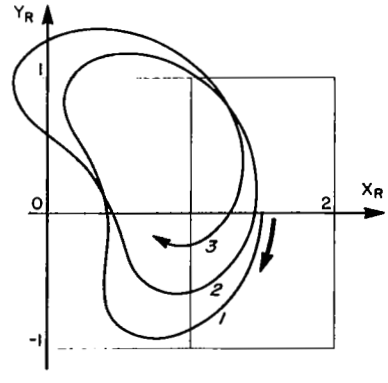

n =+16/15

$\dot{Y}_R$ =-0.96207

P/2 = 47.12

LOBE HALF-TIME ≅2.95

Figure 65

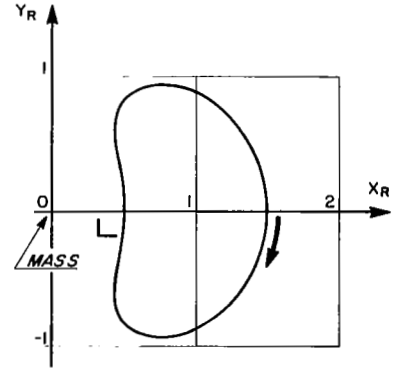

n =+1

$\dot{Y}_R$ =-0.922650

P/2 ≅ π

Figure 66

EARTH-MOON FIELD ORBITS

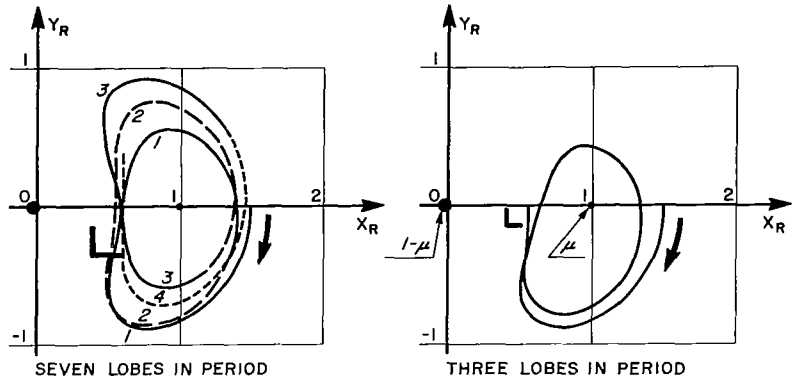

SEVEN LOBES IN PERIOD
$\dot{Y}_R$ =-0.89875
P/2 = 20.1
MEAN LOBE - HALF TIME = 2.87

Figure 67

THREE LOBES IN PERIOD
$\dot{Y}_R$ =-0.88748
P/2 = 8.39
MEAN LOBE - HALF TIME = 2.80

Figure 68

at the outer envelope and, after the loop-formation, are returning there to join the succeeding loop.

The orbits of the upper group show similarity with the Kepler orbits in their initial orbit geometry while otherwise they develop rather independently. The progressively increasing compactness of the first three orbits, however, parallels the trend that is predominant in the Kepler group (Figures 61-63).

No special effort was made to isolate periodic orbits here. To the right of the single loop orbit, two periodic orbits were encountered which are reproduced in Figures 67 and 68. The period

KEPLER ORBITS

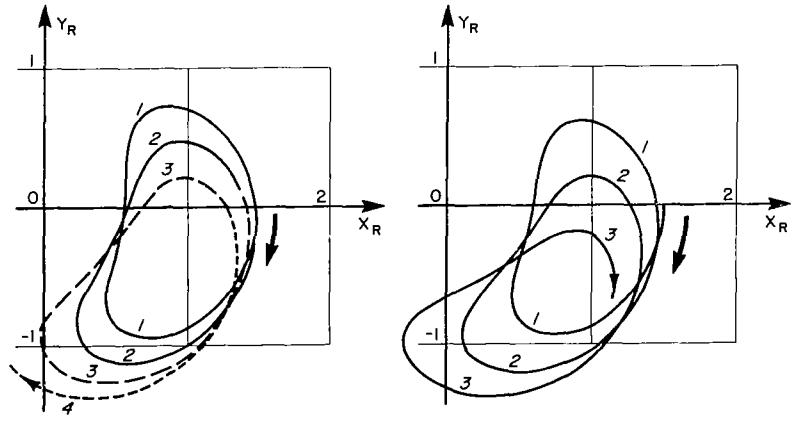

n =+23/24
$\dot{Y}_R$ =-0.89891
P/2 = 75.4
LOBE - HALF TIME = 3.28

Figure 69

n =+15/16
$\dot{Y}_R$ =-0.88726
P/2 = 50.27
LOBE - HALF TIME = 3.35

Figure 70

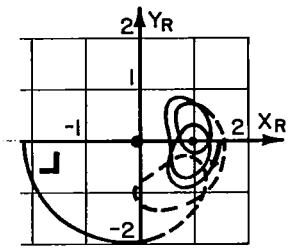

PERIODIC ORBIT
$\dot{Y}_R$ = -0.879860
P/2 = 25.98

Figure 71

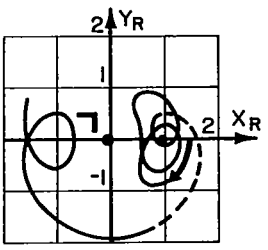

PERIODIC ORBIT
$\dot{Y}_R$ = -0.875970
P/2 = 21.71

Figure 72

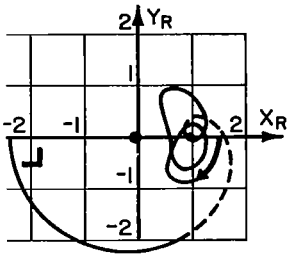

PERIODIC ORBIT
$\dot{Y}_R$ = -0.874621
P/2 = 18.25

Figure 73

covers seven loops on the earlier orbit and three loops on the latter orbit.

Next in the three-body series is a triple of closely neighbored orbits (Figures 71-73) that illustrate one possible mode of "losing a loop" in an orbital development. The loop to be lost is the one shown in dashed lines in Figure 71. This loop travels along the orbit as one progresses in the series. Figure 72 shows this loop placed at the negative X_R-axis. In Figure 73 the loop is combined with the loops present in the lunar area, without adding to their number.

Going back to Figure 71, one finds that during this progression actually two loops vanish, the second one being the mirror image of the first one. This latter one vanishes exactly with attainment of the second orbit of the triple.

This group of orbits is noteworthy for a second feature as well, viz., the partition of each orbit into a time span of lunar captivity with the remaining time spent in a more general orbit. It is interesting to see that the breakaway is in most cases accomplished with a close flyby of the Moon. The reverse procedure, the capture by the Moon, is accomplished in a similar manner.

More examples of motion alternating between two modes of flight are exhibited in the four orbits shown in Figures 74-77. In fact, the motion here alternates between a lunar satellite phase and an Earth satellite phase. The latter is understood to have zero mean angular motion with respect to the Moon as seen in the rotating system. The Earth satellite mode can well be identified when comparison is made with the Kepler orbits shown in Figures 11 and 12. So, for example, the dashed part of the orbit of Figure 74 shows the characteristics of the Kepler orbit of n = 3, as

EARTH-MOON FIELD ORBITS

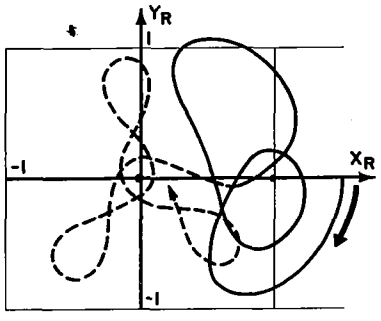

REFERENCE ORBIT
$\dot{Y}_R = -0.870$

Figure 74

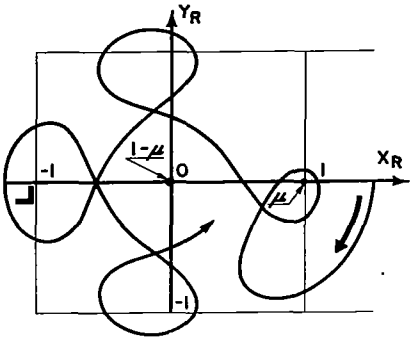

PERIODIC ORBIT
$\dot{Y}_R = -0.859495$
P/2 = 13.49

Figure 75

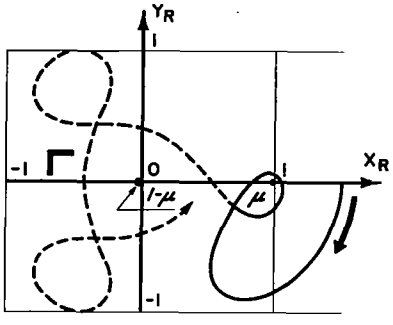

PERIODIC ORBIT
$\dot{Y}_R = -0.85716$
P/2 = 10.26

Figure 76

depicted in Figure 11, and the Earth satellite portion of the orbit in Figure 75 corresponds well to the Kepler orbit with n = 4/3, as depicted in Figure 12. The next in line (Figure 76) resembles that of n = 3/2, as seen in Figure 11, and the last of the four orbits (Figure 77) suggests the characterization by n = 5/3 for its Earth satellite portion.

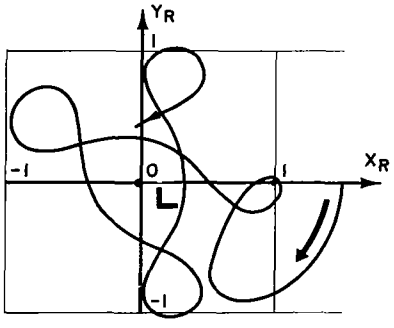

PERIODIC ORBIT
$\dot{Y}_R = -0.855166$
P/2 = 13.33

Figure 77

On all four of these orbits the lunar close approach, which triggers the transition from mode to mode, is quite pronounced.

The collision orbit, out of which the first of the four orbits is developed, is not shown here. The remaining three orbits progress toward another collision orbit. Its image is traced on Figure 81.

Since this lunar collision orbit is the last one of its nature, recorded in this report, the cases will be reviewed here. If, in the review, those orbits that reach collision after first completing a full loop (or more) around the Moon, as e.g., would be the case for an orbit between $\dot{Y}_R = -.8746$ and $\dot{Y}_R = -.8700$, are excluded here, four orbits would remain. The three collision orbits shown earlier are replotted here in Figures 78, 79, and 80. The velocity direction at which the orbits impact the Moon, especially the consistent angular progression of it from case to case, is noteworthy. Also worth noting is the relative timing of

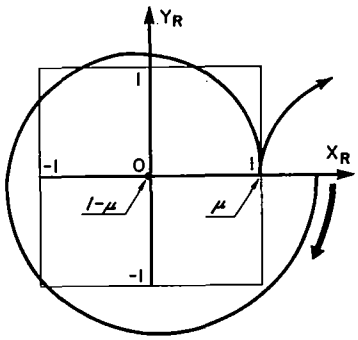

COLLISION ORBIT (MOON)

$\dot{Y}_R = -2.2190$

COLLISION TIME: 3.715

Figure 78

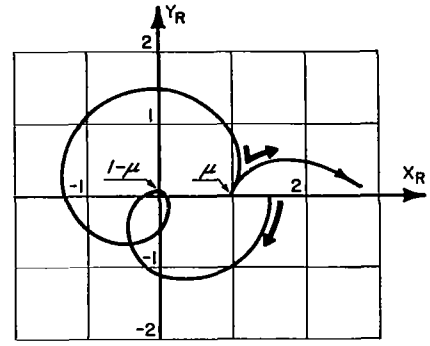

COLLISION WITH MOON

$\dot{Y}_R = -1.750$

COLLISION TIME: 5.97

Figure 79

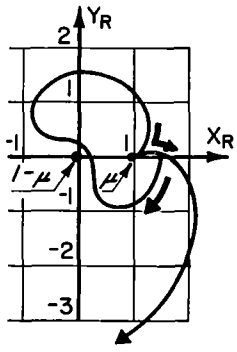

COLLISION
WITH MOON

$\dot{Y}_R = -1.1260$

COLL. TIME: 6.80

Figure 80

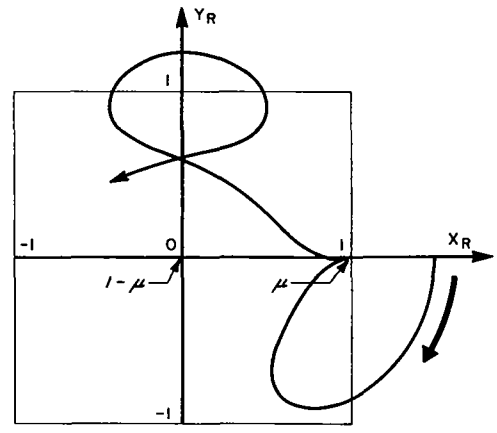

COLLISION ORBIT

$\dot{Y}_R = -0.8489$

COLLISION TIME: 4.18

Figure 81

the collision events with the last one shown not being the earliest in time, as might perhaps be suggested by the short path length.

If the significance of a collision orbit is measured by the number and variety of events that are brought about in the flyby orbits in the neighborhood of the collision orbit, then the last collision orbit is ranking highest in this respect among the four listed. As the subsequent figures (82-99) will prove, many types of orbits are packed into the space generated by the small increase of initial velocity of less than $\Delta v = 0.001$.

Figure 82 portrays a periodic orbit that, after flyby of the Moon, makes an extended excursion into the field ahead of

EARTH-MOON FIELD ORBITS

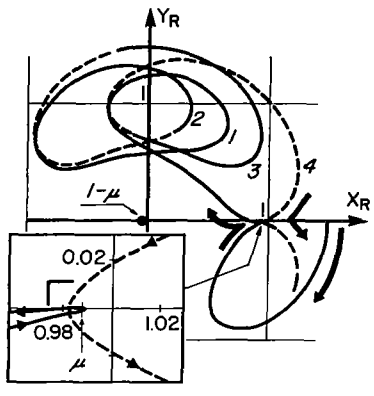

PERIODIC ORBIT
$\dot{Y}_R$ =-0.848798
P/2 = 29.70

Figure 82

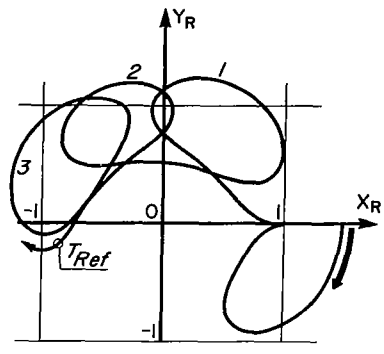

REFERENCE ORBIT
$\dot{Y}_R$ =- 0.84856
T_{Ref} = 23.4

Figure 83

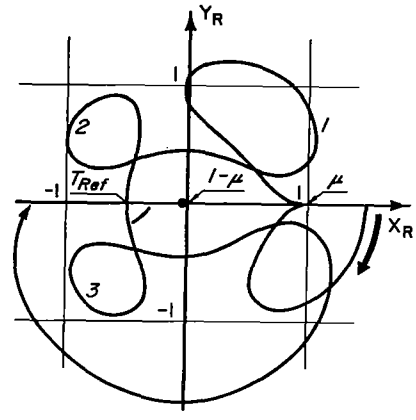

REFERENCE ORBIT
$\dot{Y}_R$ =-0.84850
T_{Ref} = 15.84
ANGLE AT T_{Ref} = 88.7°

Figure 84

the Moon. From there it returns to the Moon, crossing the X_R axis orthogonally between the two masses. The insert in Figure 82 delineates the flyby arcs in enlarged scale. In its full period, this orbit makes only one revolution about the Moon, with the sense of the revolving motion being direct. The (normalized) time period is nearly 60 units which corresponds to about 9 months in the real Earth-Moon system.

Note that the loops are numbered according to their sequence in time. So are the loops of the next six orbits. The purpose is to draw attention to the relative position of these loops and the formation through which they are going over the course of the subsequent orbits.

Figure 83 demonstrates the beginning of the formation with the loops extending forward in sequence of their numbers. On the subsequent orbit (Figure 84) loops are spaced far apart, the fourth loop extending into the lunar area. Here, also, it may be recognized that with little effort this orbit can be modified to let the crossing at $T = T_{Ref}$ be exactly orthogonal whereby a periodic orbit is obtained that encloses both Earth and Moon.

In Figure 85, the number 2 loop is coming close to the negative X_R-axis. In Figure 86, this loop is straddling the axis, cutting it at 89.4 degrees. A minute correction in the initial velocity will result in an orthogonal crossing at this place. (It is worth observing that the correction is concerned with the fifth significant digit!)

EARTH-MOON FIELD ORBITS

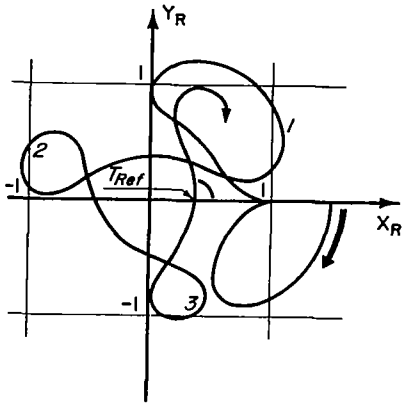

REFERENCE ORBIT
$\dot{Y}_R$ =-0.84847
T_{Ref} = 19.25
ANGLE AT T_{Ref} = 87.0°

Figure 85

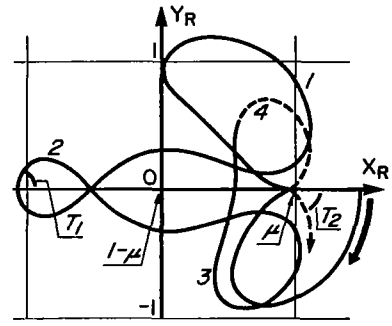

REFERENCE ORBIT
$\dot{Y}_R$ =-0.84845
T_1 = 12.9 WITH $\measuredangle$ =94.6°
T_2 = 23.0 WITH $\measuredangle$ =89.4°

Figure 86

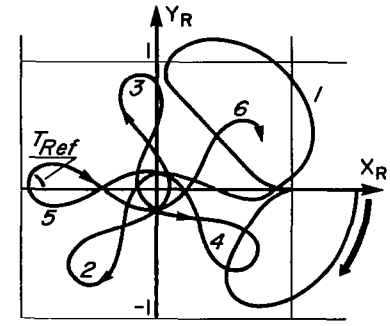

REFERENCE ORBIT
$\dot{Y}_R$ =-0.84840
T_{Ref} = 19.4
ANGLE AT T_{Ref} = 103.8°

Figure 87

In progressing to the sequent orbit (Figure 87) a number of new loops is coming into existence (six may be counted). Here again the possibility of isolating a periodic orbit is at hand, since now loop number 5 is straddling the negative X_R-axis.

Other chances for formation of periodic orbits are found between two straddling positions by the fact that the arcs linking two loops may furnish the right angle. Such a situation is approached, for example, in Figure 88 where the currently measured angle of 89.6 degrees indicates the proximity of a periodic orbit.

To introduce the orbit that now follows in the progression, another look at the orbit on Figure 82 is suggested. That orbit is the only one so far in the current group that can be considered to be of a lunar satellite mode. The orbit in Figure 89 now falls into the same classification. The topological character of this orbit is identical to that of Figure 82 insofar as it actually forms one closed loop around the Moon. This can be verified by means of the blown-up portion of the insert. The period of the present orbit, however, is much shorter than that of the former one. The character of the orbit changes drastically if the initial velocity is raised by 1/1000 of a percent as is borne out when passing from the last orbit to that of Figure 90. The new one encompasses the Earth in a wide near-circular arc after which it returns to the lunar area. This orbit is not developed to its exact periodic shape, but the angle of 88.6 degrees at the axis crossing at T_{Ref} points toward the nearness

EARTH-MOON FIELD ORBITS

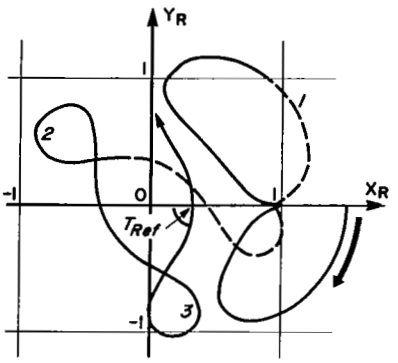

REFERENCE ORBIT
$\dot{Y}_R$ =-0.848370
T_{Ref} = 19.5 WITH $\measuredangle$ =89.6°

Figure 88

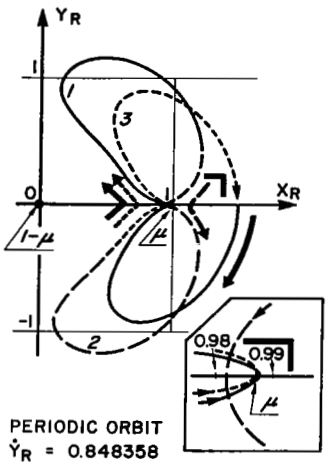

PERIODIC ORBIT
$\dot{Y}_R$ = 0.848358
P/2= 9.973

Figure 89

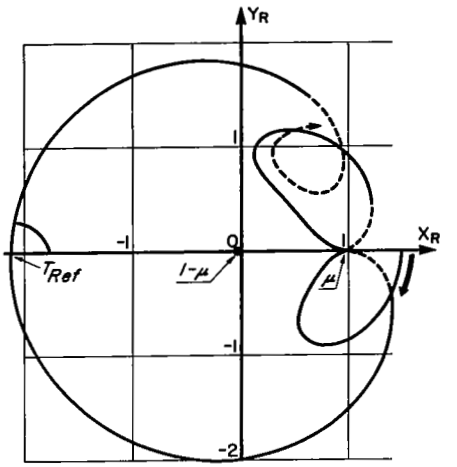

REFERENCE ORBIT
$\dot{Y}_R$ =-0.84835
T_{Ref} = 15.0 WITH $\measuredangle$ =88.6°

Figure 90

of this event. It is interesting to determine its topological classification (in the completed periodic shape). After eliminating all loops that do not encompass a masspoint, it will be found that the topological structure is that of a lemniscate.

Between the two orbits of Figures 90 and 91, there is another orbit that collides with the Moon. The collision occurs when the Moon is approached the second time. The collision is evidenced by the fact that in Figure 90 the orbit arc that makes the second pass by the Moon crosses the X_R-axis "at the left" of the Moon, i.e., between the Moon and the Earth, while in Figure 91 this crossing takes place "at the right" of the Moon.

The little loop which has formed around the Moon on the last orbit (Figure 91) will grow and decisively determine the development of the following orbits. The process shown in the next two of these orbits (Figures 92 and 93) is self-explanatory. In Figure 93, the loop referred to draws parallel to the first loop, and, as shown in Figure 94, these two loops have combined. This then is an orbit that does not enclose either of the masses. It is associated with the translunar libration point, designated L_1 in reference 1. Past this L_1-libration orbit, the second loop shows up again, now being outside and below the first loop. This is shown by the dashed curve of Figure 95. This loop "rolls away," while the progression in the series goes on.

EARTH-MOON FIELD ORBITS

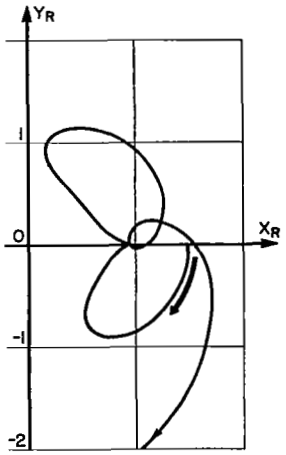

REFERENCE ORBIT
$\dot{Y}_R$ =-0.84830

Figure 91

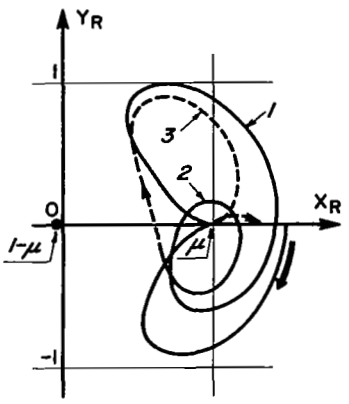

REFERENCE ORBIT
$\dot{Y}_R$ =-0.8480

Figure 92

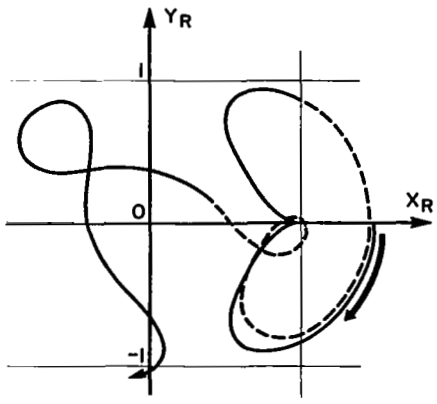

REFERENCE ORBIT
$\dot{Y}_R$ =-0.8479

Figure 93

EARTH-MOON FIELD ORBITS

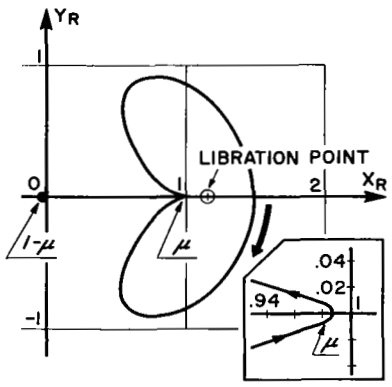

PERIODIC (LIBRATION) ORBIT
$\dot{Y}_R$ =-0.847844
P/2= 4.1952

Figure 94

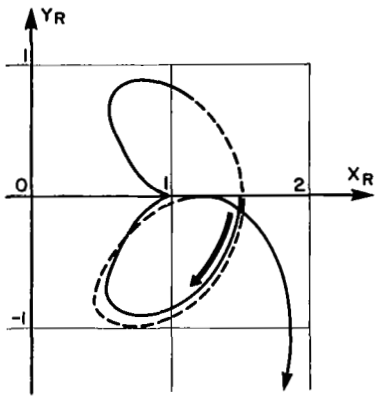

REFERENCE ORBIT
$\dot{Y}_R$ =-0.847800

Figure 95

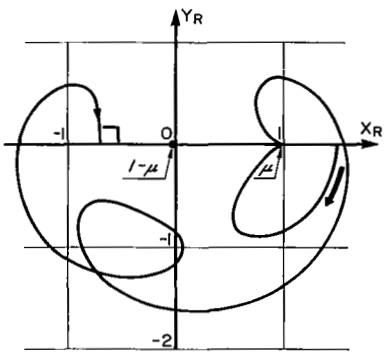

PERIODIC ORBIT
$\dot{Y}_R$ =-0.847327
P/2= 20.48

Figure 96

The general development is rather intelligible at this point in the series. A number of periodic orbits is met (Figures 96-99) which, on their Earth satellite portion, follow a pattern that is also encountered for Kepler orbits in the current velocity range. For comparison, the behavior of Kepler

EARTH-MOON FIELD ORBITS

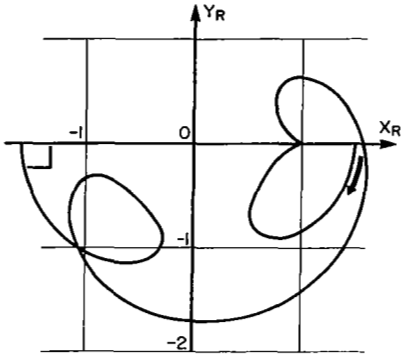

PERIODIC ORBIT
$\dot{Y}_R$ = -0.847252
P/2 = 17.31

Figure 97

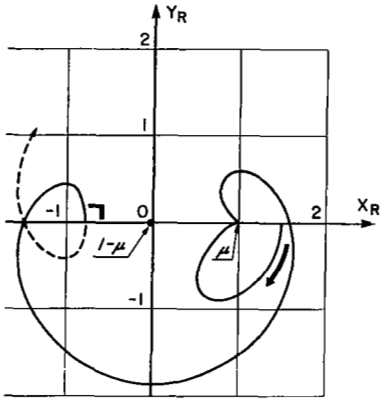

PERIODIC ORBIT
$\dot{Y}_R$ = -0.847091
P/2 = 14.11

Figure 98

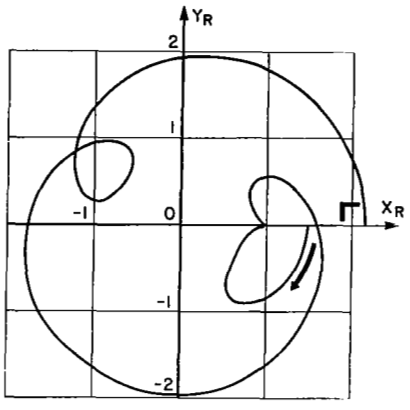

PERIODIC ORBIT
$\dot{Y}_R$ = -0.846990
P/2 = 20.36

Figure 99

orbits referred to is illustrated in Figures 100 and 101 below and 104 and 105 at the bottom of the next page. These figures demonstrate that loops are getting smaller and drifting apart.

The four orbits plotted in Figures 102, 103, 106, and 107 represent a group on its own, of which the principle of development can best be recognized by studying them in reverse direction, starting at Figure 107. This orbit shows a small loop in the lunar area, with the orbit encompassing the Earth once within its period. With a move away from this orbit to those on its left (i.e., earlier orbits), the small loop is increasing and also approaching the Moon. The "energy-gain" in this successively

KEPLER ORBITS

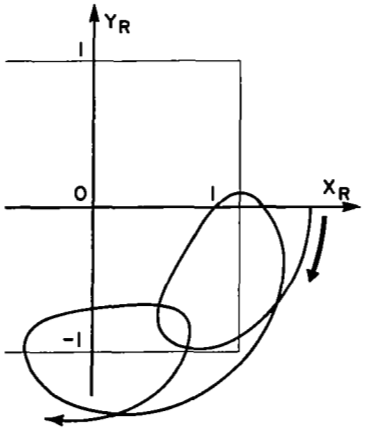

$\dot{Y}_R$ = - 0.848

Figure 100

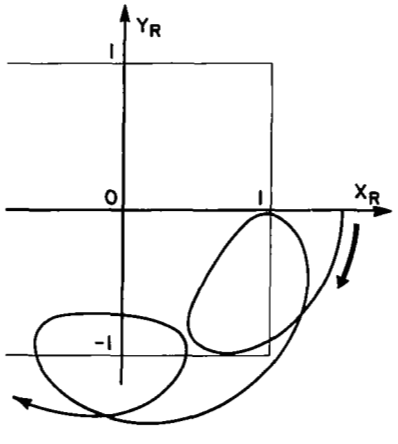

$\dot{Y}_R$ = - 0.840

Figure 101

EARTH-MOON FIELD ORBITS

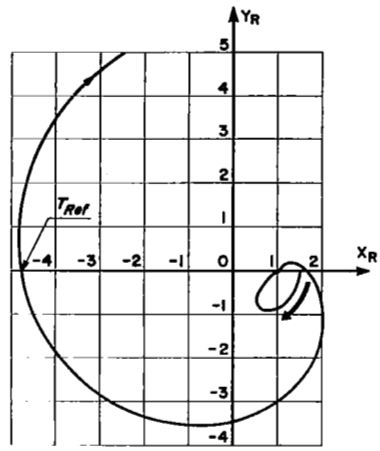

REFERENCE ORBIT
$\dot{Y}_R$ = -0.8430
T_{Ref} = 9.334

Figure 102

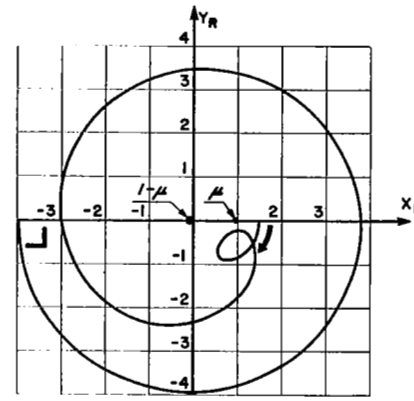

PERIODIC ORBIT
$\dot{Y}_R$ = -0.830758
P/2 = 16.12

Figure 103

closer flyby mode causes the orbits to increase their overall diameters, by which then also the number of revolutions per period about the Earth increases. The orbit of Figure 102, which is the last shown of this development, appears to be an escape orbit. (For later reference, this group will be called the "pigtail" group.)

Comparing the orbit of Figure 105 here with the orbit of Figure 107 indicates that the small loop in the three-body-orbit

KEPLER ORBITS

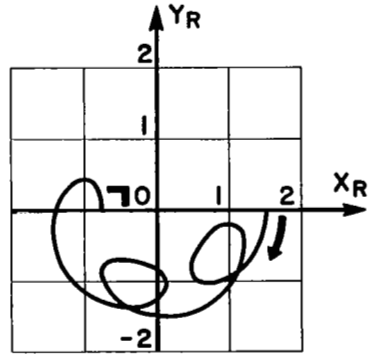

n = +5/6
Y_R = -0.830833
P/2 = 18.84

Figure 104

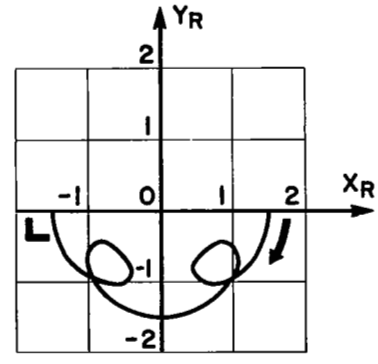

n = +4/5
Y_R = -0.813298
P/2 = 15.71

Figure 105

EARTH-MOON FIELD ORBITS

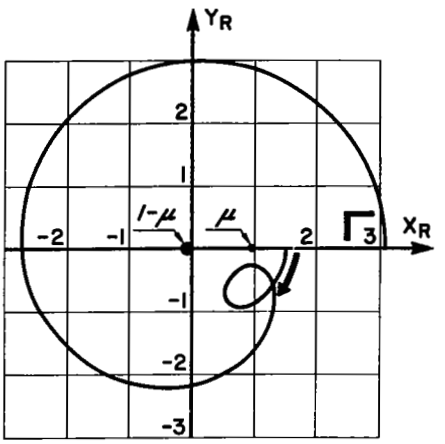

PERIODIC ORBIT
$\dot{Y}_R$ =-0.827640
P/2 = 12.88

Figure 106

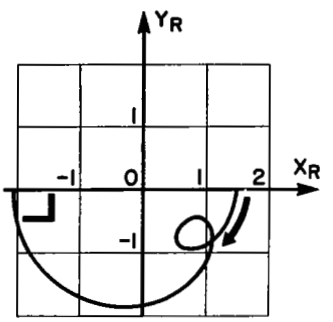

PERIODIC ORBIT
$\dot{Y}_R$ =-0.815682
P/2 = 9.460

Figure 107

is a "Kepler-characteristic," but that the effect exerted by the Moon on the loop during flyby is strong enough to change the flight pattern following the loop.

While in the velocity bracket between $\dot{Y}_R = -1.2$ and $\dot{Y}_R = -0.8$, which has just been covered, the two series compared showed a rather high disparity -- except at the very beginning of each orbit and excepting the singular case of good similarity found between the Kepler libration orbit and the single-loop lunar satellite orbit -- the orbits following from hereon exhibit a gradual restoration of comparability. Similarity will first be found in the topological structure, later also in the geometry.

Before discussing Figures 108 and 109, the progression of events may be picked up first at the Kepler series as shown in Figures 110-112. The three orbits of Figures 110-112 effectively portray the developments on both sides of a cusping orbit, with loops seen before it and smooth indentation past it. Notice that the n-value of a cusping orbit, in general, is incidental, like that of a circular orbit. It is a function of the initial distance from the origin.

Now, with respect to the three-body orbits shown in Figures 108 and 109, coordinated to the cusping Kepler orbit, one notices that the development follows the same line, but that one cannot

EARTH-MOON FIELD ORBITS

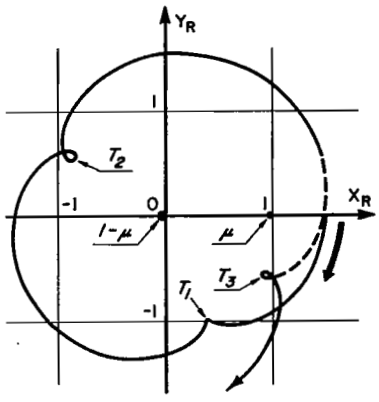

CUSPING ORBIT
$\dot{Y}_R$ = 0.7600
TIMES: T_1 = 4.02; T_2 = 12.25; T_3 = 21.50

Figure 108

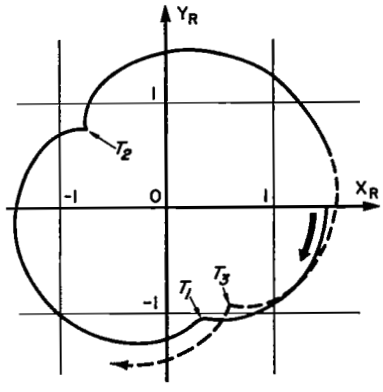

CUSPING ORBIT
$\dot{Y}_R$ = -0.7500
T_1 = 3.76; T_2 = 12.77; T_3 = 21.94

Figure 109

speak of a single cusping orbit. Rather, each of the loops that occurs over time on the three-body orbits observes its own "maturing process", thus spreading the occurrence of cusps over a range in the progression.

KEPLER ORBITS

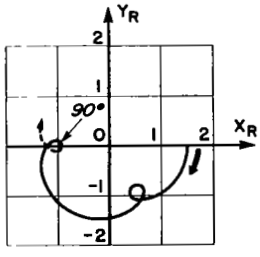

n = +3/4
$\dot{Y}_R$ = -0.78749
P/2 = 12.54

Figure 110

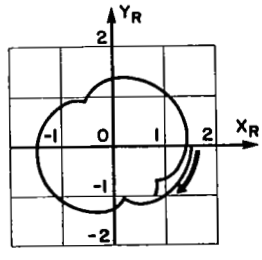

CUSPING ORBIT
$\dot{Y}_R$ = -0.75801
T_{Cusp} = 4.54; 13.62; 22.70

Figure 111

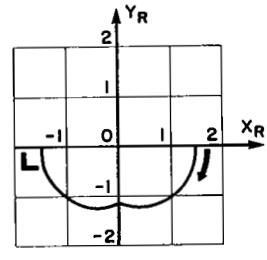

n = +2/3
$\dot{Y}_R$ = -0.74489
P/2 = 9.425

Figure 112

EARTH-MOON FIELD ORBITS

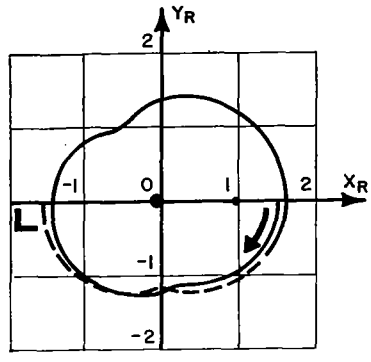

$n^* = +5/8$

$\dot{Y}_R = -.73839$

$P/2 = 27.0$

Figure 113

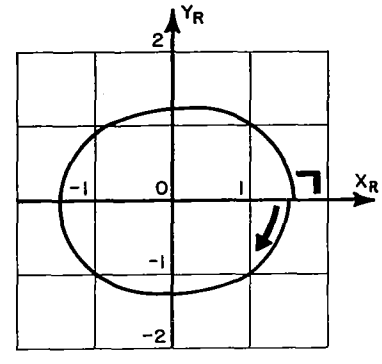

$n^* = +3/5$

$\dot{Y}_R = -.72640$

$P/2 = 17.4$

Figure 114

In Figures 113 through 120, orbit correlations and geometrical similarities are noted. In Figures 113-116, the comparability of the two series reaches the point where orbits can be correlated with respect to their n(n*)-values. Geometrical similarity is accomplished favorably in Figures 117-120. The first orbits in these figures are circular in the Kepler series and near-circular in the upper series. The second orbit (Figure 120) is of value n = +1/2 in the Kepler series; the counterpart in the upper series fails by 0.8 degree of paralleling the periodicity.

KEPLER ORBITS

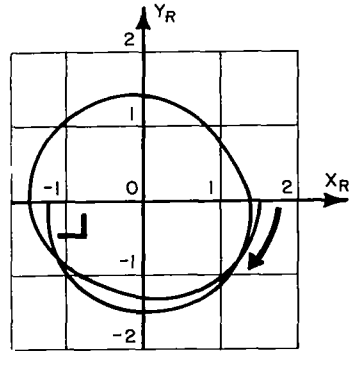

$n = +5/8$

$\dot{Y}_R = -.72390$

$P/2 = 25.1$

Figure 115

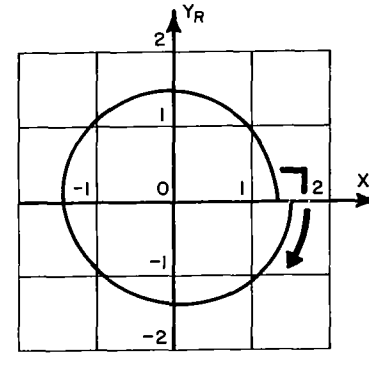

$n = +3/5$

$\dot{Y}_R = -.71136$

$P/2 = 15.7$

Figure 116

EARTH-MOON FIELD ORBITS

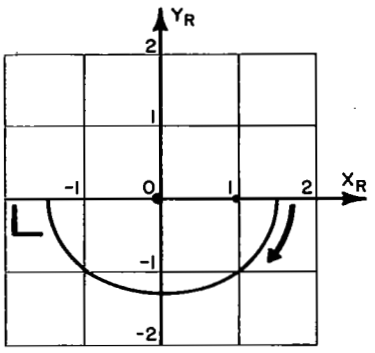

FROM: POSITIVE CIRCULAR

$\dot{Y}_R$ = -.71854

P/2 = 8.434

Figure 117

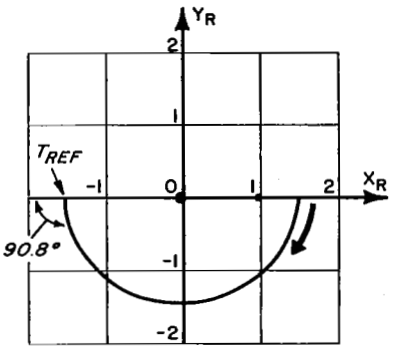

BEST APPROACH TO PERIODIC

$\dot{Y}_R$ = -.6854

T_{REF} = 7.20

Figure 118

From this point, there is a good one-to-one correspondence of Kepler orbits to those of the restricted problem of three bodies, at least as long as orbits are compared whose values of n (or n*) have low integers in the numerator and denominator. Test cases shown concern n = +5/11, +4/9, +3/7, and +2/5, all of which are plotted in Figures 124, 125, 126, and 130, with corresponding n*-cases in Figures 121, 122, 123, and 127.

The arithmetic progression in n-values would ask for the two cases of n = 1/3 and n = 0, the last one being the parabolic

KEPLER ORBITS

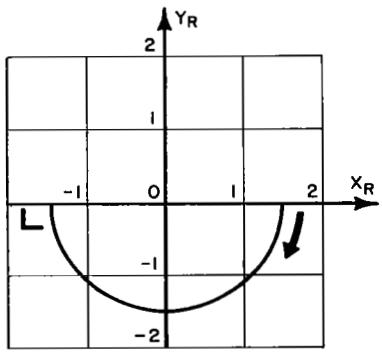

CIRCULAR (POSITIVE)

$\dot{Y}_R$ = -.68350

P/2 = 6.89

Figure 119

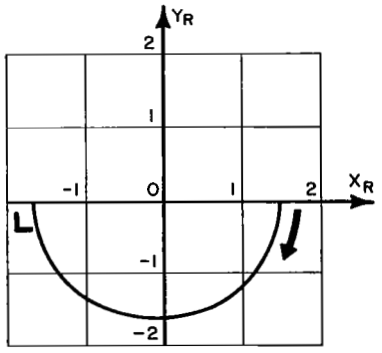

n = +1/2

$\dot{Y}_R$ = -.66133

P/2 = 6.28

Figure 120

EARTH-MOON FIELD ORBITS

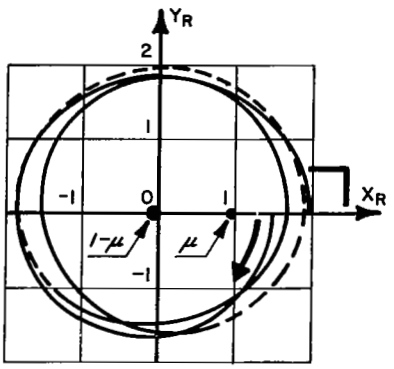

PERIODIC ORBIT

$n^* = +5/11$

$\dot{Y}_R = -0.640597$

P/2 = 34.77

Figure 121

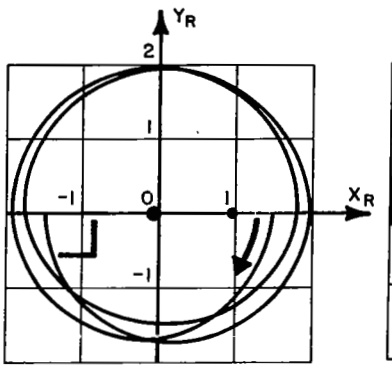

PERIODIC ORBIT

$n^* = +4/9$

$\dot{Y}_R = -0.632473$

P/2 = 28.48

Figure 122

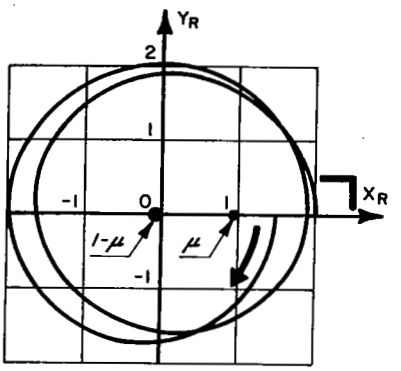

PERIODIC ORBIT

$n^* = +3/7$

$\dot{Y}_R = -0.624343$

P/2 = 22.26

Figure 123

escape orbit. The parabolic orbit was omitted because the illustration of orbit loops continuously spiralling-out is well known.

Instead, the orbit of n = 1/3 is depicted together with that of n = 1/4 (Figures 131 and 132). This serves to show the beginning development of the infinite sub-series of orbits, all associated with n-values of the type $1/\ell$ (with increasing integers ℓ) that converges toward the parabolic orbit. A parallel development holds for the E-M orbits, of which the cases of $n^* = 1/3$ and $n^* = 1/4$ are shown in Figures 128 and 129.

KEPLER ORBITS

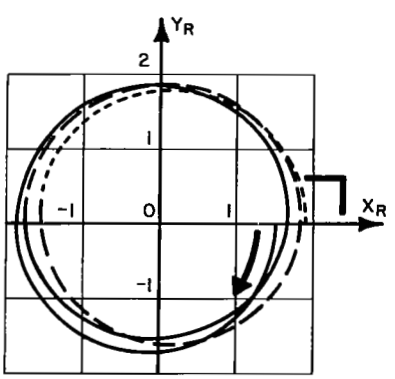

n = +5/11

$\dot{Y}_R = -0.638516$

P/2 = 34.56

Figure 124

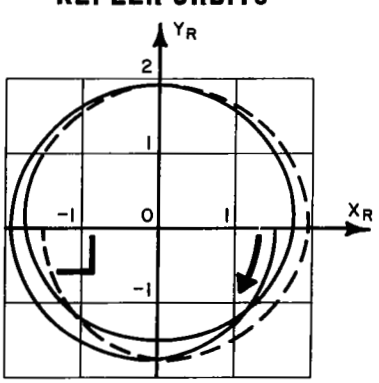

n = +4/9

$\dot{Y}_R = -0.633428$

P/2 = 28.27

Figure 125

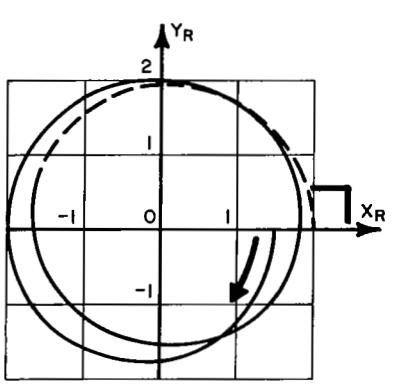

n = +3/7

$\dot{Y}_R = -0.625416$

P/2 = 21.99

Figure 126

EARTH-MOON FIELD ORBITS

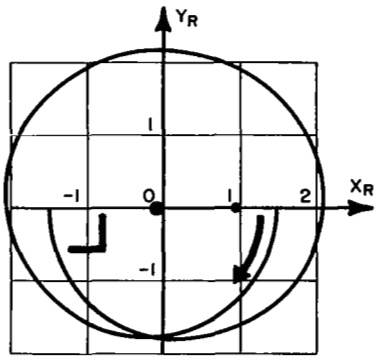

PERIODIC ORBIT

$n^* = +2/5$

$\dot{Y}_R = -0.611820$

$P/2 = 16.01$

Figure 127

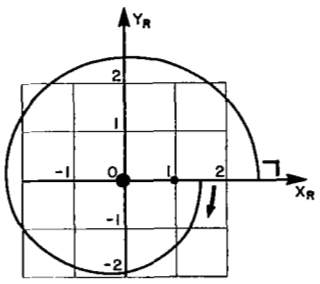

$n^* = +1/3$

$\dot{Y}_R = -0.57621$

$P/2 = 9.62$

Figure 128

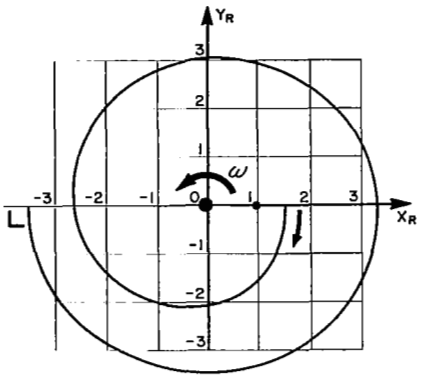

$n^* = +1/4$

$\dot{Y}_R = -0.52845$

$P/2 = 12.70$

Figure 129

Exhibiting these cases also serves to point out the similarity of this development with that observed in two groups discussed earlier. One of these is that represented by the orbits of Figures 26, 27, and 28 with n = -1/2, -1/3, -1/4 with correspondence of n = -1/2 to n = +1/4 and n = -1/3 to n = +1/5, and so forth. The second group is that spoken of as "pigtail series" and is represented in Figures 102, 103, 106, and 107.

KEPLER ORBITS

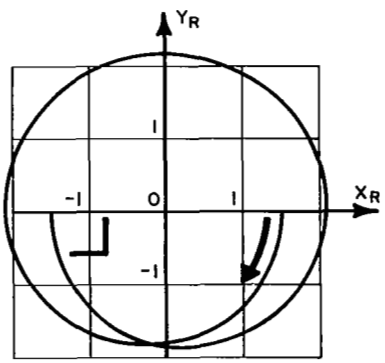

$n = +2/5$

$\dot{Y}_R = -0.610927$

$P/2 = 15.71$

Figure 130

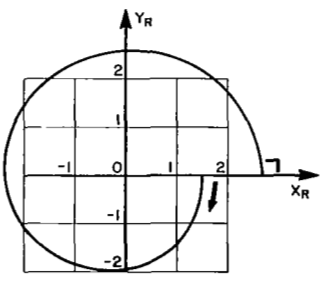

$n = +1/3$

$\dot{Y}_R = -0.57665$

$P/2 = 9.42$

Figure 131

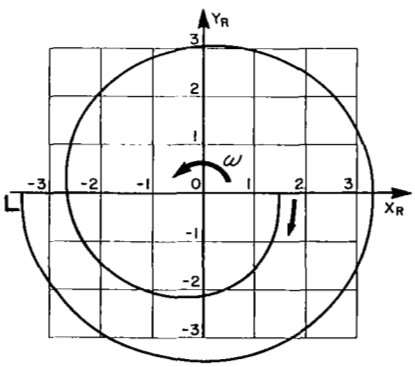

$n = +1/4$

$\dot{Y}_R = -0.53228$

$P/2 = 12.57$

Figure 132

EARTH-MOON FIELD ORBITS

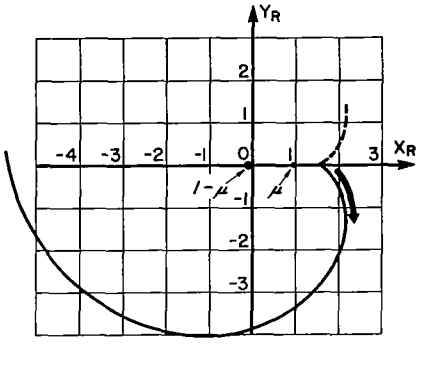

CUSPING ORBIT
$\dot{Y}_R = 0.00$

Figure 133

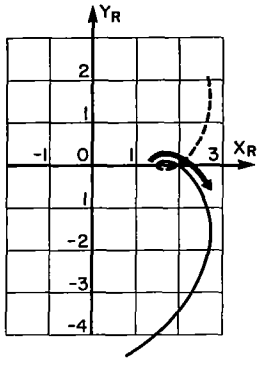

REFERENCE ORBIT
$\dot{Y}_R = +0.300$

Figure 134

The two final orbits that are presented for either series (Figures 133-136) serve to illustrate events and developments encountered in the hyperbolic range. The orbit of Figure 135 represents the only other cusping orbit there is in the Kepler series. The cusp is at the beginning of the orbit where the velocity coordinates are $\dot{X}_R = \dot{Y}_R = 0$. For better visibility of the cusp, some negative time is shown on the orbit (dashed curve). The series of the restricted problem of three bodies contains the exact counterpart to this orbit.

The orbits of Figures 134 and 136 exemplify the development the two series take after passing the previously mentioned cusping orbits. The cusps are succeeded by loops that are growing in

KEPLER ORBITS

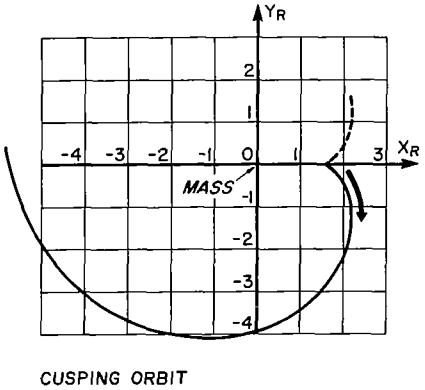

CUSPING ORBIT
$\dot{Y}_R = 0.00$

Figure 135

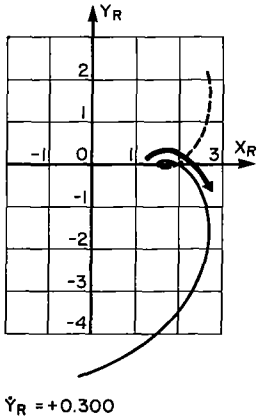

$\dot{Y}_R = +0.300$

Figure 136

size with progression of the series. The symmetry points of the loops are at the points of orbit initiation. The initial velocity is positive from now on. However, consistently, the angular motion on all these orbits will eventually reverse to the retrograde direction and remain so.

National Aeronautics and Space Administration
Electronics Research Center
Cambridge, Massachusetts, August 1968
129-04-04-06

REFERENCES

1. Szebehely, V.: Theory of Orbits, Academic Press, New York, 1967.

2. Hoelker, R.F.: Numerical Studies of Transitions Between the Restricted Problem of Three Bodies and the Problem of Two-Fixed Centers and the Kepler Problem. NASA TM-X-1465, November 1967.

3. Arenstorf, R.F.: New Regularization of the Restricted Problem of Three Bodies. Astronomical Journal, Vol. 68, No. 8, October 1963.

APPENDIX

DIFFERENTIAL EQUATIONS AND METHODS OF REGULARIZATION AND INTEGRATION EMPLOYED IN THE COMPUTATIONAL PROGRAM

1.- REGULARIZATION OF THE RESTRICTED PROBLEM OF THREE BODIES

Part 1 of the Appendix considers the equations of motion of the planar restricted problem of three bodies. The Newtonian equations of motion are regularized to eliminate singularities and to allow the analytic continuation of solutions passing through the singular points. The regularizing transformation and its development is due to Arenstorf (ref. 1).

Consider the motion of three bodies in a two-dimensional rotating system. Assume the only forces in inertial space are inverse square attractive forces acting between the bodies. Assume masses m_1 and m_2 are in circular orbits about their common center of mass and mass m_3 is sufficiently small that it does not affect the motion of m_1 or m_2.

The planar equations of motion are given in a coordinate system with origin at the center of mass of m_1 and m_2, and rotating with respect to inertial space with angular velocity such that m_1 and m_2 remain fixed on the rotating X_R axis (Figure A-1). $\underline{C}_1$ and $\underline{C}_2$ ($C_1 > 0$, $C_2 \leq 0$) are constant vectors on the X_R-axis and locate m_1 and m_2 with respect to their center of mass. The limits on C_1 and C_2 are discussed in Part 2 of this Appendix. $\underline{r}$ locates m_3 with respect to the origin; $\underline{r}_1$ locates m_3 with respect to m_1; and $\underline{r}_2$ locates m_3 with respect to m_2.

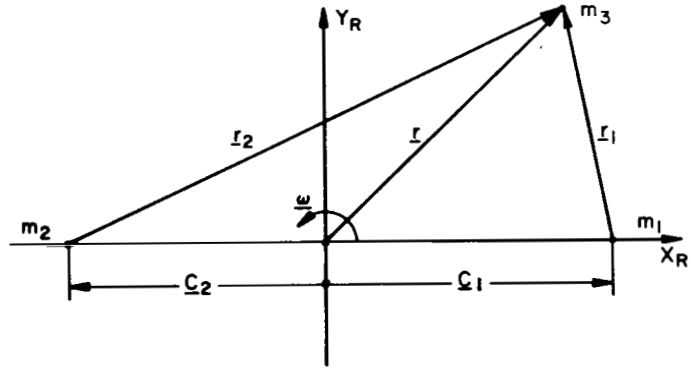

Figure. A-1

The equations of motion of m_3 in the above system are

$$\ddot{\underline{r}} + 2\underline{\omega} \times \dot{\underline{r}} - \omega^2 \underline{r} = - \frac{Gm_1}{r_1^3} \underline{r}_1 - \frac{Gm_2}{r_2^3} \underline{r}_2 \qquad (1)$$

with $\underline{\omega}$, the angular velocity of the coordinate system, directed normal to the plane of motion, and the magnitude given by

$$\omega = \sqrt{\frac{G(m_1 + m_2)}{(C_1 - C_2)^3}} \quad . \qquad (2)$$

The regularization transforms the $1/r^2$ singularities so that the new system is integrable (in a computational sense) and continuous at these points.

The normalization of the equations of motion could be carried out in the usual way. The mass unit is chosen such that the sum of masses m_1 and m_2 is unity. The unit of length is chosen such that $(C_1 - C_2)$ is unity and the unit of time is chosen such that G is unity. With these definitions, the circular angular velocity ω is also unity.

However, the regularization carried through below is done with the non-normalized equations of motion.

Transform the Cartesian coordinate system X_R, Y_R to a complex coordinate system in which the complex position vector z is given by $z = X_R + iY_R$. For simplicity of notation, denote a complex function by the subscript 1 and its complex conjugate by the subscript 2. Introduce a complex u plane such that u maps onto z by

$$z_k = f(u_k) \qquad (k = 1,2) \qquad (3)$$

where f(u) is real when u is real. This implies that $f(u_k) = f_k(u)$ $(k = 1,2)$. In terms of u and f(u), a Lagrangian for the restricted problem of three bodies is:

$$L(u_k,\dot{u}_k) = (f_1'\dot{u}_1 + i\omega f_1)(f_2'\dot{u}_2 - i\omega f_2) + \frac{2Gm_1}{\sqrt{(f_1-C_1)(f_2-C_1)}} + \frac{2Gm_2}{\sqrt{(f_1-C_2)(f_2-C_2)}} \quad (4)$$

Since it can be shown that the Lagrangian satisfies Euler's equation in terms of the u_k's and $\dot{u}_k$'s, a Hamiltonian can be obtained for the system from

$$H^* = \sum_k \dot{u}_k v_k - L(u_k,\dot{u}_k) \quad (5)$$

where v_k, the conjugate momenta, are defined by

$$v_k = \frac{\partial L}{\partial \dot{u}_k} . \quad (6)$$

H* remains constant and can be identified as twice the Jacobi constant.

Let us transform the time t to a parameter s such that

$$s = \int_o^t \frac{1}{g(u_1)g(u_2)}\, dt \quad (7)$$

where g(u) is analytic and real when u is real. g(u) is to be chosen such that (a) s is monotonically increasing with t, (b) the integral exists everywhere, and (c) s approaches a finite limit as t approaches a time of collision.

A new Hamiltonian H is now defined as

$$H = g_1 g_2 (H^* - h^*) \quad (8)$$

for which the canonical differential equations of u_k and v_k in the s domain are given by

$$u_k'(s) = \frac{\partial H}{\partial v_k(s)}$$
$$v_k'(s) = -\frac{\partial H}{\partial u_k(s)} \tag{9}$$

and h* is the value of H* defined at t = s = 0.

H becomes

$$H = g_1 g_2 \left[\frac{v_1 v_2}{f_1' f_2'} + i\omega \left(\frac{v_2 f_2}{f_2'} - \frac{v_1 f_1}{f_1'} \right) - 2G \left(\frac{m_1}{\sqrt{(f_1 - C_1)(f_2 - C_1)}} + \frac{m_2}{\sqrt{(f_1 - C_2)(f_2 - C_2)}} \right) - h^* \right] \tag{10}$$

and it can be seen from Eq. (8) that H = 0 for all s.

f(u) and g(u) are chosen such that H contains no transcendental or algebraic functions and no singularities which cause difficulties in the integration of Eq. (9).

Make

$$f(u) - C_1 = s^2(u) \tag{11}$$

$$f(u) - C_2 = r^2(u) \tag{12}$$

where r(u) and s(u) are rational functions with zeros of first order and common poles. A suitable choice for r(u) and s(u) is

$$r(u) = \frac{1}{2}\sqrt{C_1 - C_2}\left(u + \frac{1}{u}\right)$$
$$s(u) = \frac{1}{2}\sqrt{C_1 - C_2}\left(u - \frac{1}{u}\right) \tag{13}$$

In the u-plane, mass m_1 is located at $u = \pm 1$ and mass m_2 is located at $u = \pm i$. Eq. (3) is then a 4-to-1 mapping of the u-plane into the z-plane since $\pm u$ and $\pm u^{-1}$ are solutions for the same z.

From Eq. (12), whenever s(u) or r(u) are zero, f'(u) must also be zero. Therefore it is required that g(u) has first-order zeros corresponding to the zeros of f'(u), r(u), and s(u). Furthermore, g(u) must satisfy conditions (a), (b), and (c) of Eq. (7).

A choice for g(u) is

$$g(u) = uf'(u) = r(u)s(u) \tag{14}$$

Finally, H in its simplest form is

$$H = u_1v_1u_2v_2 + i\omega(u_2v_2f_2g_1 - u_1v_1f_1g_2) - 8G(m_1r_1r_2 + m_2s_1s_2) - g_1g_2h^* \tag{15}$$

Once the initial conditions in the z-plane have been transformed to the u-plane, Eq. (9) may be integrated together with

$$t = \int_o^S g(u_1)g(u_2)\, ds \tag{16}$$

and the result transformed back to the z-plane.

The only singularities occur when $u = 0, \infty$; but from Eqs. (12) and (13), these correspond to $z = \infty$ and hence $t = \infty$. The singularities therefore present no problem in the actual computation of a trajectory.

For reasons to be discussed in the following section, the equations were integrated by power series. Integration of Eqs. (9) and (16) by series in u and v is impractical, thus motivating the development and integration of a system of equations explicitly independent of u and v.

Define the parameters

$$\begin{aligned}
\alpha_1 &= r(u_1) \\
\beta_1 &= s(u_1) \\
\gamma_1 &= 2f(u_1) - (C_1 + C_2) \\
\delta_1 &= \alpha_1\beta_1 \\
\varepsilon_1 &= u_1 v_1 \\
\mu_1 &= \varepsilon_2 - i\omega\delta_2(\gamma_1 + C_1 + C_2) \\
\eta_1 &= \alpha_2\beta_1
\end{aligned} \tag{17}$$

Differentiating with respect to s (' denotes d/ds), making use of Eq. (9), and appending Eq. (16) results in

$$\begin{aligned}
\alpha_1' &= \beta_1\mu_1 \\
\beta_1' &= \alpha_1\mu_1 \\
\gamma_1' &= 4\delta_1\mu_1 \\
\delta_1' &= \gamma_1\mu_1 \\
\varepsilon_1' &= i\omega[4\varepsilon_1\delta_1\delta_2 - \varepsilon_2\gamma_1(\gamma_2 + C_1 + C_2)] \\
&\quad + 8G(m_1\eta_1 + m_2\eta_2) + 4\gamma_1\delta_2 h^* \\
\mu_1' &= \varepsilon_2' - i\omega[\gamma_2(\gamma_1 + C_1 + C_2)\mu_2 + 4\delta_1\delta_2\mu_1] \\
\eta_1' &= \beta_1\beta_2\mu_2 + \alpha_1\alpha_2\mu_1 \\
t' &= 4\delta_1\delta_2 \ .
\end{aligned} \tag{18}$$

It should be noted that each equation, except for t, represents two equations: one equation for the real part and one equation for the imaginary part. Furthermore, closed form recursion formulas for the coefficients of the series may be developed, thus eliminating numerical differentiation.

The initial conditions for Eqs. (18) are developed from Eq. (17). Eq. (13) is solved for one of the four values of u in terms of the initial conditions defined in the z plane. v is determined from Eq. (6) for regions "not too close" to a mass from

$$v_1 = \frac{\delta_1}{u_1}\left[2\dot{z}_2 - i\omega(\gamma_2 + C_1 + C_2)\right] \tag{19}$$

For close approaches to a mass Eq. (19) is not useful since $\dot{z} \to \infty$. Under this condition Eq. (15) suggests that the initial conditions be derived from u, h*, and one component of v. Since H = 0, the other component of v can be easily found.

2.- REDUCTION OF THE REGULARIZED THREE-BODY PROBLEM TO THE REGULARIZED TWO-BODY PROBLEM.

It is possible to reduce the regularized equations for the restricted problem of three bodies to the regularized equations for the Kepler problem provided that care is taken in the limiting process.

Let us assume that $m_1 = 0$. Since C_1 and C_2 are measured with respect to the center of mass, which now corresponds to m_2, a first assumption would be that both C_1 and C_2 were zero. With this assumption, however, the regularizing equations would become invalid.

If m_1 were zero and m_2 were finite, the equation for the center of mass would require that C_2 be zero, but it would allow C_1 to be arbitrary. To preserve the regularized equations, it is necessary that C_1 be any positive non-zero number. This definition accounts for the limits of C_1 and C_2 defined in Part 1 of the Appendix.

The Kepler problem, in a three-body sense, can thus be thought of as the motion of a third mass about two other masses, one of which has a mass value zero and is located at a non-zero distance from the center of mass.

3.- NUMERICAL INTEGRATION METHOD AND OUTPUT CONTROL

In problems of computing families of trajectories, some thought must be given to the amount and nature of the computed output. It is essential that a minimum of computed points display all the required information in a form which can be easily assimilated. These considerations -- and the ones below -- motivated the tailoring of the equations so that they may be integrated by series.

In a numerical integration, if no control is placed on the number of lines of output, each integration step is bounded only by the constraints of computational accuracy. By specifying the number of lines of output for any trajectory, additional problems are encountered. For example, if too many points are computed, some would have to be selectively suppressed, while if not enough are computed, more points would have to be generated. The problem then is to develop a scheme which will print out an entire trajectory in a fixed number of lines and relate all the desired information.

One of the first complications arises since the integration is done in the s domain. In the t domain, the integration starts at $t = 0$ and terminates at $t = T_{max}$, where T_{max} is a specified terminating time. However, from Eq. (7) one can see that the value of s corresponding to T_{max} is not unique but rather a function of the trajectory on which it is computed. Hence, T_{max} must be retained as the terminating condition and any scheme based on s cannot be used without knowledge of the trajectory. Furthermore, attempting to relate the number of lines to intervals in the time domain would require undesirable iterations in the s domain in order to find the value of s relating to a particular time t.

It was resolved that the trajectory had to be computed in its entirety to obtain sufficient information such that the output could be generated within a fixed number of lines. The series approach was considered to be the most desirable method of integration for several reasons. First, the trajectory could be integrated faster and could use larger steps than with the standard Runge-Kutta techniques. Truncation error in the series could be handled in an open-loop fashion by adjusting the interval length of the truncated series such that the remainder is bounded. Second, in an interval, the series gives a functional representation of the trajectory, in contrast to the discrete representation given by a Runge-Kutta method. Furthermore, in a system of coupled differential equations, once the coefficients of the series solution of a single variable are known, that variable may be treated independently of the solutions of the other variables of the system.

A FORTRAN IV program was written in double-precision which integrates Eq. (18) by series. It was found that the absolute values of the coefficients were divergent, so the series were truncated after 15 terms. The applicable interval length for the truncated series was determined such that the sum of the absolute values of the last three terms of each series was less than 10^{-10}.

Since this will not guarantee convergence, the problem of accuracy was attacked by a number of numerical comparison tests using a Runge-Kutta method. However, in a practical way, the accuracy was checked most reliably with the Kepler cases, since these, for uniformity of procedures, are calculated by the very same computational program that computes the restricted three-body cases.

For the purposes of the output control, the coefficients and the respective interval lengths are saved until the entire trajectory is computed.

With respect to the control of the distribution of points to be printed out, it is desired to have a scheme that assigns a judiciously denser output to events which occur on a smaller time scale than to events which occur on a larger time scale, and yet be flexible enough to enhance the dominant characteristics of the entire trajectory.

Having computed the trajectory in its entirety, assigning an approximately equal number of printout lines to each interval results in a spread of printouts that is not only economical but also satisfies the requirements of illustration. For it is the very process of finding the interval length of the series and determining the corresponding interval of time as a function of the location on a trajectory (the last equation of Eq. (18)) which relates the weighting of the printouts to the dynamical properties of events on the trajectory.

4.- MAPPING GEOMETRY

In this part of the Appendix the geometry of the mapping of the z-plane into the u plane will be described, with special attention given to the images of the X_R and Y_R-axes in the u plane. Reference to this will be made in the following section with regard to the isolation of periodic orbits and collision orbits.

Insight of the mapping of z into u is gained by investigating the equations mapping u into z. Writing u in polar form,

$$u = Re^{i\theta} \tag{20}$$

the mapping of u into z is given by Eq. (3)

$$z = f(u)$$

$$= \left(\frac{C_1 - C_2}{4}\right)\left(R^2 + \frac{1}{R^2}\right)\cos 2\theta + \frac{1}{2}\left(C_1 + C_2\right)$$

$$+ i\left(\frac{C_1 - C_2}{4}\right)\left(R^2 - \frac{1}{R^2}\right)\sin 2\theta \qquad (21)$$

Note first that R and R^{-1} map into the same z. Thus each z will give two values of R except when $R = R^{-1} = 1$.

Mapping the line $Y_R = 0$ into u maps the X_R-axis into u. $Y_R = 0$ for $\theta = n(\pi/2)$ $(n = 0,1,2,3,4)$ or $R = 1$. A mapping of the X_R-axis is given in Figure A-2.

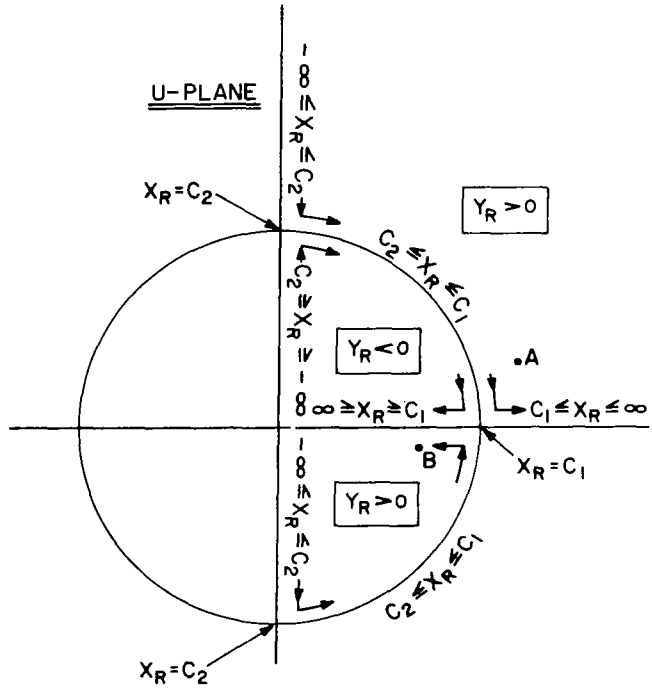

Figure. A-2

a) For $\theta = 0$

$$C_1 \leq X_R \leq \infty \longrightarrow 1 \leq R \leq \infty \quad \text{or} \quad 1 \geq R \geq 0$$

b) For $\theta = \pi/2$

$$C_2 \geq X_R \geq -\infty \longrightarrow 1 \leq R \leq \infty \quad \text{or} \quad 1 \geq R \geq 0$$

c) For $R = 1$

$$C_1 \geq X_R \geq C_2 \longrightarrow 0 \leq \theta \leq \frac{\pi}{2}$$

The symbol $\longrightarrow$ means the mapping of z into u. Also the limits written to the left of X_R map into the limits written to the left of R or θ and limits written to the right of X_R map into limits written to the right of R and θ.

The Y_R axis (not shown in Figure A-2) can be mapped from $X_R = 0$ by

$$\cos 2\theta = -2\left(\frac{C_1 + C_2}{C_1 - C_2}\right) \frac{1}{R^2 + \frac{1}{R^2}} \quad . \tag{22}$$

For the interval $0 \leq \theta \leq \pi/2$, several observations can be made:

(1) If $|C_1| = |C_2|$, Y_R maps onto a 45^o line.

(2) At $R = 0$ and $R = \infty$, the mapping of Y_R is asymptotic to the 45^o line.

(3) If $|C_1| < |C_2|$, $\theta < 45^o$

(4) If $|C_1| > |C_2|$, $\theta > 45^o$

Thus the entire X_R axis and the entire Y_R axis are mapped into the first quadrant of u. After mapping the two half-planes $Y_R \geq 0$, $Y_R \leq 0$ into u for $0 \leq \theta \leq \pi/2$

(1) $0 \leq Y_R \leq \infty \longrightarrow 1 \leq R \leq \infty$

(2) $-\infty \leq Y_R \leq 0 \longrightarrow 0 \leq R \leq 1$

it can be seen that the entire z plane is mapped into the first quadrant of u. z may be mapped into the other three quadrants to complete the one-to-four mapping by rotations and reflections of the first quadrant as z maps into -u by a 180° rotation of the first quadrant into the third, and z maps into $\pm u^{-1}$ by reflecting the first and third quadrant about the real u axis. Care must be taken in reflecting since the mappings for (1) and (2) are interchanged as shown in the fourth quadrant of Figure A-2. Finally, in the u plane, m_1 is located at $u = \pm 1$ and m_2 is located at $u = \pm i$.

It may be noted that as long as C_1 and C_2 do not simultaneously go to zero, the mapping has significance and its general properties are unchanged. Therefore the mapping is applicable to the Kepler problem as well as the three-body problem, provided the limiting process is as described in Part 2 of the Appendix.

Trajectories in the z plane can now be related to trajectories in the u plane.

5.- TECHNIQUE OF ISOLATING PERIODIC ORBITS AND COLLISION ORBITS

In all cases considered in this report, the initial conditions are such that the trajectory starts on the X_R-axis with velocity orthogonal to the X_R-axis. If the trajectory has the above initial conditions, a necessary and sufficient condition that Eq. (1) be periodic is that the trajectory return orthogonal to the X_R-axis. The problem of isolating periodic trajectories can thus be characterized to finding the magnitude of the initial velocity such that the trajectory returns orthogonal to the X_R-axis on the n^{th} crossing of that axis. The crossing criterion is established to distinguish different types of periodic trajectories.

The orthogonality condition is satisfied if $\dot{X}_R$ vanishes at the n^{th} crossing. From Eq. (19):

$$\dot{z}_1 = \frac{1}{2}\left[\delta_1\varepsilon_2 - i\omega\delta_2\delta_1\left(\gamma_1 + C_1 + C_2\right)\right] \Big/ \left(\delta_1\delta_2\right) . \qquad (23)$$

The condition that $\dot{X}_R$ vanishes is that the real part of the numerator of Eq. (23) vanishes. This condition simplifies to

the vanishing of the real part of $\delta_1\varepsilon_2$, since γ_i (the imaginary part of γ) vanishes on the X_R axis. Using this condition not only isolates orthogonal crossings, but it also isolates collisions since δ (=g(u) from Eq. (17)) vanishes identically at a collision.

Therefore, the vanishing of the real part of $\delta_1\varepsilon_2$ on the n^{th} crossing of the X_R-axis isolates orthogonal crossings and collisions.

Let ϕ equal the real part of $\delta_1\varepsilon_2$ at the n^{th} crossing of the X_R-axis. The following discussion is directed to the orthogonal crossing, but may be applied to the collision without loss of generality.

The iterative process on the initial velocity first establishes the sign of the derivative of the initial velocity with respect to ϕ. The initial velocity is varied such that the absolute value of ϕ is decreasing until a change of signs in ϕ occurs. If the sign of the derivative defined above changes signs prior to ϕ changing signs, the initial velocity is iterated such that the absolute value of ϕ is minimized. This process isolates the trajectory which best approaches an orthogonal crossing and shows that an orthogonal crossing may not exist for the neighborhood of the iterated initial velocities.

If ϕ changes signs, it is assumed that an orthogonal crossing exists and that an upper and lower bound on the initial velocity has been established. The iteration reduces the interval in such a way that $|\phi|$ approaches zero and is terminated when the variation of the initial velocity is in the eleventh significant digit.

This then describes the general approach to isolating periodic and collision trajectories. The remainder of this discussion will be devoted to the methods used to determine a crossing of the X_R-axis and the method of evaluating ϕ.

6.- CROSSING OF THE X_R-AXIS

The criteria for determining a crossing of the X_R-axis will now be established. In the z plane, a crossing is indicated by a change of signs of Y_R. Therefore, let changes of signs of a parameter or parameters, as yet unspecified, indicate a crossing. Second, the parameters to be tested are constrained to those integrated in Eq. (18) or a combination thereof. Third, the testing should be done only on those points computed in the initial integration of the trajectory. These points are then the initial points and final points of an interval, the final point

being identical to the initial point of the following interval. Fourth, the parameters to be tested should also indicate the possibility of a collision. And fifth, the tests should be as few as possible and the parameters as simple as possible.

From Eqs. (17) and (21), γ would appear a suitable candidate as a testing parameter. γ_i, as stated previously, is directly proportional to X_R and changes of signs in γ_i would indicate the crossings. The value of γ_r (the real value of γ) relative to C_1 or C_2 at the crossing would indicate the proximity to a collision.

However, γ does not prove to be a very good parameter for the following reasons. Consider in the u plane a single interval with the initial point in the first quadrant outside the unit circle and the final point in the fourth quadrant inside the unit circle (points A and B in Figure A-2). It can be seen that both points lie in a mapping of $Y_R > 0$ and hence γ_i would not indicate a crossing, while, in fact, either two crossings or a collision occurred. Furthermore, γ_i could not indicate a collision, since, in a strict sense, a collision trajectory touches the X_R-axis at only a single point and does not cross it, except for collisions symmetric about the X_R axis. Therefore, γ is excluded as a useful parameter.

Although the u plane does exhibit the proper number of crossings, we have attempted to remain explicity independent of u. Utilizing u at this point would have required twice the number of equations and thus twice the computation time to arrive at the same result as derived by the method presented below.

If one had attempted to rationalize the choice of parameters in Eq. (17), one would conclude at first that η was chosen because it simplified the differential equations and the recursion formulas. However, in the light of the past discussion, η has a much greater significance which is brought out in the mapping of u, in polar form, into the η plane.

$$\eta = \eta_r + i\eta_i$$

$$= \frac{C_1 - C_2}{4}\left(R - \frac{1}{R}\right) + i\,\frac{C_1 - C_2}{2}\sin 2\theta \qquad (24)$$

Note first that η_r changes signs whenever the trajectory crosses the unit circle ($R = 1$) in the u plane and, second, that η_i changes signs whenever the trajectory passes through a phase angle $\theta = n(\pi/2)$ $(n = 0,1,2,3,4)$ in the u plane. From the

mapping of the X_R axis in the u plane, it can be seen that the change of signs of η_r or η_i corresponds to a crossing of the X_R axis. Third, and equally significant, the simultaneous vanishing of η_r and η_i corresponds to a collision.

The mapping in effect takes the X_R-axis mapped in the u plane onto the η_r axis and the η_i axis and maps the four mass points in u into the origin in η.

The problem of the double crossing encountered by γ_i is now taken care of by the simultaneous changing of signs by η_r and η_i in the same interval. However, additional refinements must be made in this type of situation since the change of signs only occurs at the endpoints of the interval. For the purposes of counting crossings, isolation of the n^{th} crossing, or isolation of a collision, it is necessary to subdivide the interval until either the crossings lie in separate subintervals or until a numerical collision is established. A numerical collision is defined when the length of η lies within a circle of radius 10^{-8} and is then treated as a true collision. The crossing of the origin of η thus motivates the count of one crossing for a collision.

Once the interval containing the n^{th} crossing has been determined, it is simple to determine by iteration the subinterval length for which the η_r or η_i series, or both, go to zero, thus locating the X_R-axis. Knowing this subinterval length, ϕ can be computed directly and the isolation of periodic or collision trajectories can proceed as described in Part 5 of this Appendix.

REFERENCE

1. Arenstorf, R.F.: New Regularization of the Restricted Problem of Three Bodies. Astronomical Journal, Vol. 68, no. 8, 1963.